DEVELOPMENT OF SIMPLIFIED LIMIT ANALYSIS TECHNIQUES AND THEIR APPLICATION TO SHIP STRUCTURE COMPONENTS

SAKIB LUTFUL MAHMOOD

Development of Simplified Limit Analysis Techniques and their Application to Ship Structure Components

By

Sakib Lutful Mahmood ©

A thesis submitted to the School of Graduate Studies

in partial fulfillment of the requirement for the degree of

Master of Engineering

August 2010

Faculty of Engineering and Applied Science

Memorial University of Newfoundland

St. John's Newfoundland Canada

ABSTRACT

In this thesis, the m_α- tangent method is implemented in conjunction with an elastic modulus adjustment procedure (EMAP) and an algorithm has been proposed for limit load estimation. This technique is applied to a number of ship structure components possessing different kinematic redundancies. By specifying spatial variations in the elastic modulus, numerous sets of statically admissible and kinematically admissible stress and strain distributions are generated, and both lower and upper bound limit load multipliers are obtained. Utilizing the lower and upper bound multipliers, accurate limit loads of ship structure components are then determined using the m_α- tangent method. Furthermore, a reference volume correction for regions of peak stresses is incorporated to ensure lower bound limit loads in all the linear elastic iterations. Results are compared with the inelastic finite element results and available analytical solutions.

Lower bound limit loads for ship structure components are also determined based on a single linear elastic finite element analysis by invoking the concept of kinematically active reference volume in conjunction with the m_α-tangent method. The method enables rapid determination of lower bound limit loads for ship structure components by taking their kinematically inactive volume into consideration. This method is applied to a number of ship structure components possessing different percentages of inactive volume. Results are compared with the corresponding inelastic finite element results, and available analytical solutions.

ACKNOWLEDGEMENT

I would like to express my heartiest and sincerest gratitude to my supervisors, Dr. M. Haddara and Dr. R. Seshadri for their intellectual guidance, tireless support, constructive suggestions, inspiration, and close supervision throughout the entire period of my M.Engg. program.

I would like to thank my course instructors of Memorial University Dr. R. Seshadri, Dr. S. Adluri, Dr. G. George, Dr. G. Rideout and Dr. K. Munaswamy for their valuable lectures and course materials which directly helped me in my research.

I would like to extend my acknowledgements to my friends in the Asset Integrity Management Research Group for their valuable help and support.

I would like to thank Dr. C. Daley, Professor Ocean and Naval Architectural Engineering; Dr. R. Adibiasl, AMEC NSS Limited; and Dr. W. D. Reinhardt, Atomic Energy of Canada Limited (AECL), for their valuable technical feedback and encouragement.

I also would like to thank Ms. Heather O'Brien, Canada Research Chair's office, Ms. Moya Crocker, and Ms. Mahoney Colleen, Graduate office, Faculty of Engineering and Applied Science for their administrative assistance during the course of my program.

Last but not the least, I owe my deepest thanks to my wife, my daughter, and my beloved parents. At the end, I feel to thank the almighty for setting this M.Engg. mission as one of the assignment of my indeterminate life span.

TABLE OF CONTENTS

LIST OF TABLES

LIST OF FIGURES

NOMENCLATURE

E	Elastic modulus
L_1 ,L_2	Lengths of the bars
m	Exact limit load multiplier
m_L	Classical lower bound limit load multiplier
$m_{L,Bar}$	Classical lower bound limit load multiplier for the two bar model
$m_{L,Comp}$	Classical lower bound limit load multiplier for the component
m^0	Upper bound limit load multiplier
m_2^0	Upper bound multiplier based on variable flow parameter
m_{Bar}^0	Upper bound limit load multiplier for the two bar model
m_{Comp}^0	Upper bound limit load multiplier for the component
m_{ref}^0	Kinematically active reference volume based upper bound multiplier
m_U	Classical upper bound limit load multiplier
m_α	Multiplier Alpha
m_α^T	m_α-tangent multiplier
m_{NFEA}	Inelastic FEA based multiplier
$m_{Analyt.}$	Analytical multiplier
P	Arbitrary applied load
P_L	Lower bound limit load
q	Elastic modulus adjustment parameter

R^0 Ratio of $\frac{m^0}{m}$

R_α Ratio of $\frac{m_\alpha}{m}$

V_R Kinematically active reference volume

V_D kinematically inactive volume

V_T Total volume

σ_{eq} von Mises equivalent stress

$\sigma_{\max}$ Maximum von Mises equivalent stress

σ_{ref} Reference stress

σ_y Yield strength

ε_{eq} Equivalent strain

ζ Iteration variable, Ratio of $\frac{m^0}{m_L}$

ζ_f Value of ζ after blunting of peak stresses at the end of any linear elastic analysis

ζ_i Value of $\frac{m^0}{m_L}$ after any linear elastic analysis

Subscript

eq equivalent

ref reference

Superscript

0	statically admissible
i	iteration number

Abbreviation

bar	Two bar Structure
Comp	Component
EMAP	Elastic Modulus Adjustment Procedure
FEA	Finite Element Analysis

Abbreviation

ASME	American Society of Mechanical Engineers
FEA	Finite Element Analysis
FEM	Finite Element Method
NFEA	Nonlinear Finite Element Analysis
TBM	Two Bar Model

CHAPTER 1

INTRODUCTION

1.1 General Background

The primary objective in designing a component or structure is to ensure its ability to perform its intended function at minimum capital and operational cost. Therefore it is important to design components by taking into account all failure modes that the component may experience. It is also necessary to periodically assess the "integrity" of components, and structures and, by this process, an estimate of the remaining life of critical components can be obtained.

Beams, frames, plates and stiffened panels are the structural building blocks of marine vehicles. Nowadays limit analysis has been found to be a useful tool for designing and

maintaining ship structure components. Ship design rules are also changing from the traditional working stress approach to new rules which consider plastic limit states. The rationale behind this development is the realization that structural materials tend to have large reserve strength capacity after they have yielded and prior to their eventual plastic collapse. The use of some portion of the reserve strength capacity for resisting loads will result in lighter structures which are easier to fabricate. Moreover, determination of limit loads for ship structure components is an important factor in the integrity assessment for their safe operation.

Limit load analysis is performed in order to determine the limiting load at which the structure or component will collapse (uncontained plastic flow or plastic collapse). Lower bound limit loads are especially relevant from a design point of view since they provide a guaranteed margin of safety against load controlled plastic failure modes, or the related primary stress limits contained in the design codes (ASME 2007). The concept of reference stress (Webster and Ainsworth 1994), used extensively in the United Kingdom in high temperature integrity assessment procedures and inelastic fracture evaluations (Ainsworth 2000, British Standards 1994), is related to the limit load.

Periodical assessment of the structural integrity of ship structures is also an important issue for the safety of ship structure components. The assessment tool should be simple enough so that it can be used by marine engineers who are not structural analysis experts. Furthermore, any analysis implemented in a decision support system must be capable of producing results on a rapid basis. If a tool requires a significant amount of time to

perform calculations then the damage scenario could become much more severe than the computed value by the time of computation. Therefore the tools need to be able to return results as soon as the damage has been identified.

1.2 Background for Plastic Design Methods in Ships

Conventionally, limit loads are determined either analytically using bounding theorems, or typically by using the finite element method. Plasticity theory, as a branch of mechanics, was born at the end of the 19th century, when Tresca (Calladine 2000) formulated the first yield condition for metals. In the 1950s Drucker, Greenberg and Prager formulated two fundamental theorems (lower bound and upper bound theorems) of limit analysis for elastic-perfectly-plastic materials (Drucker, Prager and Greenberg, 1952). Analytical limit load solutions for simple beam and plate structures are obtained on the basis of these theorems. Drucker presented the first paper about the advantages and disadvantages of plastic design methods (Drucker 1957). The ultimate strength of a ship structure was first evaluated by Caldwell (1965) using rigid plastic mechanism analysis. Smith (1977) extended the method of Caldwell and proposed a method for the collapse analysis of a box girder subjected to longitudinal bending. Yao and Nikolov (1991) developed analytical solution for the progressive collapse of a hull girder subjected to longitudinal bending. Paik and Mansour (1995) developed a simple formulation for predicting the ultimate strength of ships. Paik and Pedersen (1996) extended the method of Yao and Nikolov (1991) by assuming three plastic collapse modes and validated their results using non-linear FEA. Paik *et al.* (1999) studied the ultimate strength of a stiffened

panel subjected to uniaxial compression and developed design equations for the ultimate strength of a plate subjected to different types of loading. Daley *et al.* (2001) proposed roof type collapse mechanism and derived the analytical solution for the collapse pressure of a beam fixed at two ends. Hong and Amdahl (2007) extended the roof type collapse mechanism and proposed a double diamond type collapse mechanism.

In the sixties numerical methods started to be used with the support of new computing technology. The first routines permitted only lower bound analysis on the basis of elastic methods but quite soon they included plasticity and geometric non-linearity. The most frequently used approach to obtain a limit load is to perform an elastic-plastic analysis with no strain hardening. Inelastic finite element analysis (FEA) is an economic alternative to full scale experimental tests. However, applications of elasto-plastic analysis to the ultimate longitudinal strength analysis of a ship's hull are very few (ISSC, 1997). The difficulties arise mainly from the need to carry out analyses in an iterative and incremental form. Since this method always operates at the convergence limit, it tends to be relatively inefficient, i.e. many steps are required to obtain a good estimate of the limit load. Moreover the enormous computational time required for the analysis is expensive and produces a large amount of output data that has to be interpreted properly in order to make practical sense. Numerical difficulties can also be encountered when the calculated deformations become large, as plastic hinges form. Elements may be subjected to shear locking (Borrval, 2009) due to the amount of deformation itself. Another difficulty that may be encountered is volumetric locking (Xia and Zhang, 2009). Therefore, a simplified method such as that proposed by Smith (1976) is usually applied.

Yao (1996) determined the capacity of individual ship structural members, up to and beyond their ultimate strength, by considering four cases : (a) Elastic (No Buckling), (b) Elastic-Perfectly-Plastic (No Buckling), (c) Elastic-Critical plastic and no strength reduction after buckling, and (d) The actual behavior.

The development of alternative methods that can be used for limit load prediction in a simple and more direct manner was therefore of great value to engineers. Schulte presented the concept of skeletal points in an attempt to obtain the deflection of beams subjected to creep (Schulte 1960). The method of Treffz is a powerful tool in elasticity to estimate the lower-bound and upper-bound values of the potential energy functional of a given system in equilibrium. Mura and coworkers (Mura and Lee, 1963 and Mura and Rimawi, 1965) extended this idea to the theory of plasticity (assuming an elastic-perfectly-plastic material model). It was demonstrated that the statically and kinematically admissible multipliers are actually extreme values of the same functional under different constraint conditions (Mura and Rimawi, 1965). The theorems proposed by them are more general than the classical theorems in limit load analysis since they allow the use of general stress and strain fields. Later, Sacchi and Save (1968) proposed an approximate analysis procedure for a three-dimensional rigid-perfectly-plastic continuum derived from the Mura and Lee (1963) variational method. Zyczkowski combined analytical methods with numerical approaches such that there is no clear boundary between analytical techniques and numerical procedures (Zyczkowski 1981).

Seshadri and Fernando introduced the concept of reference nodes (r-nodes) for the purpose of determining the reference stress and limit load of mechanical components and structures on the basis of two linear elastic finite element analyses (Seshadri and Fernando 1992). This approach is simple and less time consuming than the conventional non-linear finite element analysis. Simonsen has combined analytical, empirical and numerical routines in order to analyze the plastic behavior of a ship during grounding (Simonsen 1997). He studied the plastic resistance of the basic ship structure components like a bulkhead, girder, transverse frame, stiffeners and plating. Naar examined the usefulness of the redistribution node (r-node) method as applied to the ship grounding events (Naar 2000).

From a linear elastic finite element analysis, numerous sets of statically and kinematically admissible stress distributions can be generated and lower and upper bounds of limit loads can be obtained. The closer the elastically generated stress distribution approximates the fully plastic ones, the more accurate the limit load estimates will be. The Elastic Modulus Adjustment Procedure (EMAP) can generate statically admissible stress fields and kinematically admissible strain fields which enable calculation of both lower and upper bound limit loads during successive number of linear elastic iterations. Jones and Dhalla (1981) first used the elastic modulus adjustment procedure to classify the clamp-induced stresses in a thin-walled pipe. Seshadri and Fernando (1992) proposed the r-node method using elastic modulus adjustment procedure for the determination of lower-bound limit loads of mechanical components and structures. An attempt has also been made to obtain accurate limit loads using the smallest number of linear elastic

iterations. Seshadri and Manglaramanan (1997) developed the m_α-method on the basis of two linear elastic FEAs by 'leapfrogging' to a limit state. This determines limit loads based on two linear elastic iterations. This method overcomes most of the limitations of R-Node method. However the method does still have one limitation. The limitation is that the value of m_α becomes imaginary for components with high stress concentrations. To improve the convergence towards the actual limit load during successive elastic iterations Adibi-Asl *et al.* proposed a "variable q" scheme (Adibi-Asl *et al.* 2006). Claudia et. al. (2007) investigated the applications and limitations of iterative modulus variation procedures combined with linear elastic analysis to calculate lower bounds of collapse loads for complex frame geometries.

Seshadri and Adibi-Asl (2007) developed a simplified limit load determination technique using the reference two-bar structure. Seshadri and Hossain (2009) proposed a method called the m_α-tangent method, which enables lower bound limit load determination for mechanical components and structures based on single linear elastic analysis. However, extensive investigation in the literature shows that the reference volume correction in the m_α-tangent method is still left as a scope for future research.

In this thesis an algorithm has been developed which ensures faster and proper convergence of the m_α-tangent method towards the accurate limit load multiplier in subsequent linear elastic iterations. An attempt has also been made to incorporate the reference volume correction as an additional feature to the m_α-Tangent method and to

determine the lower bound limit load for ship structure components based on a single linear elastic analysis. The proposed methods are under the category of 'service limit state' as defined by the Society of Naval Architects and Marine Engineers (Ship design and Construction, 2003).

1.3 Objectives of the Research

The aim of the present work is to develop robust and simplified methods for designing and integrity assessment of ship structures. The main set of objectives of this thesis are to:

1. Make implicit reference volume and peak stress corrections utilizing the elastic modulus adjustment procedure (EMAP).
2. Identify the kinematically active volume based upper bound multiplier from a single linear elastic analysis.
3. Develop a robust limit analysis algorithm by combining the m_α-tangent method with the EMAP.
4. Improve the accuracy of the lower bound limit load multiplier towards the exact multiplier for ship structure components based on the proposed algorithm.
5. Evaluate sufficiently accurate lower bound limit load multiplier for ship structure components based on a single linear elastic analysis which is achieved by incorporating reference volume correction with the m_α-tangent method.

1.4 Scope of Research

During local plastic action, plastic flow is confined to a sub-region of the total volume and the upper bound multiplier would therefore depend on the volume of the sub-region. Therefore limit load multipliers may be significantly overestimated if it is based on the total volume. Proper identification of kinematically active volume and peak stress is an important step in the evaluation of an accurate limit load multiplier. In this thesis, an attempt has been made to eliminate the kinematically inactive volume and peak stresses existing in the elastic stress field while performing iterative analysis and single linear elastic analysis.

From a design point of view, lower bound limit loads provide a guaranteed margin of safety against load controlled plastic failure modes. Therefore improvement of the accuracy of lower bound limit load estimation towards the exact limit load has great engineering value. EMAP establishes an inelastic-like stress field by modifying the local elastic modulus in order to obtain the necessary stress redistribution in the collapse state. Numerous sets of statically admissible and kinematically admissible distributions can be generated in this manner, which enable calculation of accurate limit load multipliers for ship structure components. In this thesis, an effort has been directed to develop an algorithm which is able to estimate sufficiently accurate lower bound limit loads for ship structure components at a minimum number of linear elastic iterations.

In this thesis, reference volume correction is incorporated into the m_α-tangent method, as an additional feature, and the method is applied to the estimation of lower bound limit loads of ship structure components based on a single linear elastic analysis. This method can also be explored as a powerful tool for structural integrity assessment of in-service ship structure components, and to evaluate their fitness for service, because of its ability to return results rapidly.

1.5 Organization of the Thesis

This thesis is composed of nine chapters. The first chapter addresses the general background, objectives and the scope of the proposed research work. The chapter also covers a brief literature review of existing limit load estimation methods.

Chapter 2 presents a brief review and application of analytical limit analysis techniques and their limitations. The chapter covers bounding theorems in plasticity and the concept of limit load multipliers. The chapter also covers the limit analysis of beams and plates based on the bounding theorems. Stress based design of components and structures are based on elastic analysis, elastic-plastic analysis, and limit analysis. In this chapter stress categorization guidelines (The ASME Boiler and Pressure Vessel (B&PV) Code Section III, 2007) are also provided which relate to the development of methods in the upcoming chapters.

Chapter 3 discusses upper bound multipliers and classical lower bound multipliers along with a review of extended variational theorems in limit analysis and a distributed parameter that characterizes the degree of collapse at a given location. This chapter also includes the evolution of the m_α-tangent method, characteristics of the m_α-tangent, explanation of peak stress in the context of m_α-tangent construction and two bar trajectory, and graphical representation of the m_α-tangent method in a two dimensional space.

Chapter 4 presents the notion of kinematically active reference volume, estimation of a reference volume based upper bound multiplier from the m_α-tangent construction and an implicit reference volume correction technique in EMAP.

Chapter 5 contains the description of different ship structure components, their finite element models, boundary conditions and loading. It also includes discussion of ANSYS 11.0 non-linear finite element analysis, its solution options and solution convergence.

Chapter 6 presents the proposed algorithm for faster and proper convergence of iterative EMAP which can estimate accurate limit loads of ship structure components. The proposed method generates statically admissible stress fields and kinematically admissible strain fields using EMAP. The method evaluates limit load multipliers using the m_α- tangent method in each iteration which rapidly converges to the exact limit load multiplier after a relatively small number of linear elastic iterations. A number of example

problems are worked out to demonstrate the algorithm of the method, and the results are verified by comparing them with those obtained from the conventional analytical and numerical methods.

Chapter 7 discusses the proposed kinematically inactive volume correction as an additional feature of the m_α- tangent method in order to obtain lower bound limit load multiplier based on a single linear elastic analysis. A number of example problems are worked out to demonstrate the inactive volume and peak stress correction and to show the lower bound nature of the m_α^T-multiplier. Results are verified by comparing them with those obtained from the conventional analytical and numerical methods.

Chapter 8 summarizes and concludes the findings of the present work. This chapter also identifies original contributions of this thesis along with some guide lines for future work.

CHAPTER 2

LIMIT ANALYSIS AND STRESS BASED DESIGN

2.1 Introduction

Simplified methods of limit analysis can be employed in structures for which the exact collapse load is difficult to compute. Collapse analyses are based on theorems which establish lower bounds and upper bounds for the collapse load. The true collapse load is always larger than or equal to the lower bound collapse load and it is always smaller than, or equal to the upper bound collapse load. The collapse load is thus bracketed between the upper and lower bounds.

In the era prior to the introduction of finite element analysis, these theorems were in common use in analysis and design methodologies. It was considered sufficient, for all

practical purposes, to estimate the limit load of engineered structures that were below the true value. Obtaining a lower bound estimate of limit loads was seen by the designers as a pragmatic way of ensuring safe designs. However, when estimating power requirements for metal cutting or metal forming, for instance, the upper bound values of loads were considered to be appropriate.

The classical lower and upper bound theorems of plasticity still play an important role in engineering design, although today's powerful computational tools can be used to great effect. In the following sections these two bounding theorems are described and applied to beams and plates in order to present the concept of limit analysis.

Elastic stresses are divided into different categories and allowable limits are imposed for each of the categories and their combinations in order to guard against distinct type of failures. Different categories of stresses and their role in component design are also discussed this chapter. The elastic stress categorization concept is utilized to develop robust limit analysis techniques which are explained in the later chapters of the thesis.

2.2 Bounding Theorems in Plasticity

The main objective of the limit load analysis is to estimate the limit load multiplier at the impending plastic limit state of a body. However, for complicated problems it may be difficult to find the exact limit load. Therefore, based on the extremum principles of limit load analysis, the bounding theorem is employed to estimate the limit load directly

without considering the entire loading history. There are two approaches in bounding theorems: the equilibrium approach for lower bound estimates and the geometry approach for upper bound estimates. The load at plastic collapse is termed the limit load of the structure. In the 'service limit state' design material nonlinearity is included by assuming a perfectly plastic material model, while the geometric nonlinearity is not taken into account (Ship Design and Construction, 2003).

2.2.1 Lower Bound Theorem

The statement of the classical lower bound theorem is as follows (Callandine, 2000):

"If any stress distribution throughout the structure can be found, which is everywhere in equilibrium and balances the external loads and at the same time does not violate the yield condition, those loads will be carried safely by the structure"

Therefore, the load estimated by the lower bound theorem will be less than, or at most equal to, the exact limit load. In the lower bound theorem, the equilibrium equations (statically admissible stress field) and yield condition are satisfied without considering the mode of deformation of the structure. This theorem is explained by an example in section 2.3.1(a).

2.2.2 Upper Bound Theorem

The upper bound theorem states that (Burgreen 1975):

"When the work done by the external loads is equal to, or greater than the internal work done by deformation in the fully plastic region of a structure, the external loads will represent an upper bound to the load of the structure".

In processes such as metal forming and metal cutting, it is necessary to determine the load that is capable of performing the given operation. Determination of limit loads using the upper bound theorem ensures that the limit load estimates obtained can cause "plastic flow" in the component. This theorem is explained by an example in section 2.3.1(b).

2.3 Application of Lower and Upper Bound Theorems

2.3.1 Determination of Limit Load for a Uniformly Loaded Fixed End Beam

Let us consider a both end fixed beam subjected to uniformly distributed load as shown in Figure 2.1. From the free body diagram as shown in Figure 2.1(b) it is evident that, the two end moments are acting due to fixity which restricts the deflection of the beam at the ends.

(a) Schematic diagram (b) Free body diagram

Figure 2.1 Fixed end beam

(a) Limit load based on lower bound theorem

For this beam there are two equilibrium equations, $\sum F_y = 0$ and $\sum M = 0$. But from the free body diagram it is evident that number of unknowns is four. Thus it is indeterminate by two (4-2) degrees. Therefore three plastic hinges are required for plastic collapse. With an increase of the load, first two plastic hinges will form at A and B locations and hence M_A and M_B will be equal to the plastic moment (M_P). However the structure will not collapse, it will just loose its indeterminacy. With further increase of load, third plastic hinge will from at the maximum bending moment location (when $M_{max} = M_P$) and eventually the structure will fail.

Assume, at the beginning, an arbitrary load q has been applied to the structure. Now the bending moment at the B location is,

$$-M_B = R_A L - M_A - \frac{qL^2}{2} \tag{2.1}$$

If we want to find the bending moment at any location x,

$$M_x = R_A x - M_A - \frac{qx^2}{2} \tag{2.2}$$

In order to find the exact limit load from the lower bound theorem, it is required to identify the maximum bending moment location. Consideration of any other location will render limit load lower than the exact limit load. Maximum bending moment occurs at the location (x_D) where $\frac{dM_x}{dx} = 0$. Differentiating Eq. (2.2) with respect to x and setting the left hand side to zero,

$$x_D = \frac{R_A}{q} \tag{2.3}$$

Substituting x_D into Eq. (2.1),

$$M_{max} = \frac{R_A^{\,2}}{2q} - M_A \tag{2.4}$$

Let us gradually increase the load up to collapse load (q_c) when M_{max} will become M_P. By this time, M_A and M_B have also definitely become M_P (because the plastic hinges at the fixed ends form before the hinge forms at collapse location). Now substituting M_{max}, M_A, and M_B with M_P, and substituting q by q_c in Eq. (2.1) and Eq. (2.4),

$$R_A = \frac{q_c L}{2} \tag{2.5}$$

$$M_p = \frac{R_A^{\,2}}{2q_c} - M_P \tag{2.6}$$

Now by substituting R_A from Eq. (2.5) into Eq. (2.6), we can obtain the exact collapse load expression,

$$q_c = \frac{16 M_P}{L^2} \tag{2.7}$$

This is the expression for limit load based on the lower bound theorem.

(b) Limit load based on upper bound theorem

The upper bound theorem states that, if any arbitrary displacement pattern of the structure is assumed during collapse, it will estimate either higher or exact collapse load for the applied load pattern. This is because, for an applied load, the structure will follow that deformation pattern which requires minimum potential energy. Any other assumed

displacement pattern will require more potential energy and thus ends up rendering a higher collapse load.

Let us assume an arbitrary displacement pattern (for Figure 2.1(b)) during plastic collapse as shown in Figure 2.2.

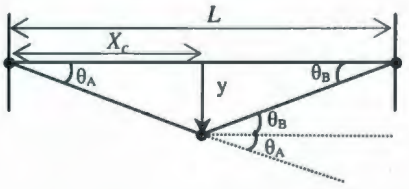

Figure 2.2 Collapse mechanism of a fixed end beam

$$\text{Total work done by the external load} = \int_0^{X_c} q\frac{yx}{X_c} + \int_{X_c}^{L} q\frac{y(L-x)}{L-X_c} \tag{2.8}$$

$$\text{Total internal work} = M_P\theta_A + M_P\theta_B + M_P(\theta_A + \theta_B) \tag{2.9}$$

Here
$$\theta_A = \frac{y}{X_c},\ and\ \theta_B = \frac{y}{L-X_c} \tag{2.10}$$

Equating external work (Eq. (2.8)) with internal work (Eq. (2.9)) will give,

$$q = \frac{4M_P}{X_c(L-X_c)} \tag{2.11}$$

From Eq. (2.11) it is clear that for a different assumption of displacement pattern, X_c will be different. Therefore for the correct displacement pattern, X_c will be such that q is minimum, and q will be minimum when $(\frac{dq}{dX_c} = 0)$,

$$X_c = \frac{L}{2} \tag{2.12}$$

Substituting y from Eq. (2.12) to Eq. (2.11),

$$q_c = \frac{16M_P}{L^2} \tag{2.13}$$

This is the expression for the exact limit load based on the upper bound theorem.

For a rectangular beam of width b and height h, the expression for plastic moment is,

$$M_P = \frac{1}{4}\sigma_y bh^2 \tag{2.14}$$

Considering force per unit area, $$P_c = \frac{q_c}{b} = \frac{4\sigma_y h^2}{L^2} \tag{2.15}$$

A fixed end beam with length, L = 508 mm; height, h = 25.4 mm and width, w=25.4 mm is modeled. The modulus of elasticity of the material is 206.85 GPa and the yield strength is 206.85 MPa. The beam is subjected to uniformly distributed load of 1 MPa. Comparison of the analytical result and the inelastic FEA result is shown in Table 2.1.

Table 2.1 Limit load of a fixed end beam (MPa)

Analytical	Inelastic FEA
2.069	2.154

2.3.2 Determination of Limit Load for Rectangular Plates

Let us consider a simply supported plate (shown in Figure 2.3), with side lengths *a* and *b*, subjected to uniformly distributed load. In the limiting state, the straight yield-lines divide the plate into four symmetric parts as shown in Figure 2.3.

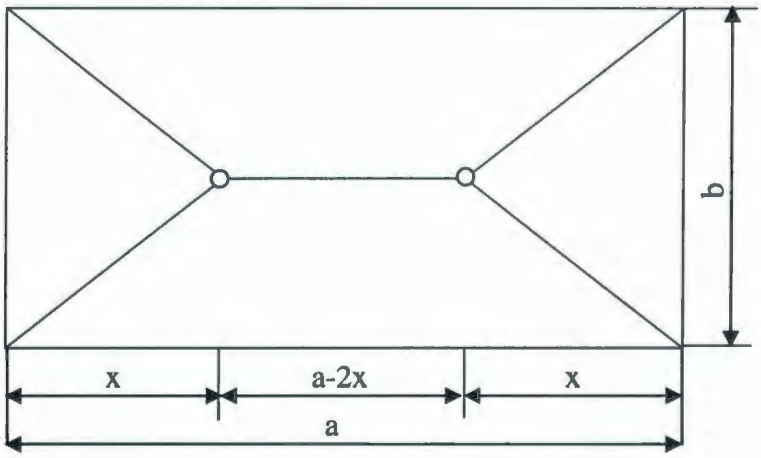

Figure 2.3 Simply supported rectangular plate with plastic hinge lines

The equation of the internal moments and the moments of external uniform load about the supported edges render the following equations, for triangular and trapezoidal sections respectively:

$$\frac{1}{6}qbx^2 = M_p b \tag{2.16}$$

$$\frac{1}{8}qb^2(a-2x)+\frac{1}{12}qb^2x = M_p a \tag{2.17}$$

Method 1: Direct kinematic solution (Hinge Method)

Dividing Eq. (2.16) by Eq. (2.17), we obtain the quadratic equation for determining the distance from the short edges of the plate:

$$x^2+\frac{b^2}{a}x-\frac{3b^2}{4}=0 \tag{2.18}$$

$$\text{i.e. } x = \frac{b}{2}\left[-\frac{b}{a} + \sqrt{\left(\frac{b^2}{a^2} + 3\right)}\right] \tag{2.19}$$

Substituting x in Eq. (2.17) gives the limit load expression as,

$$q = \frac{24 M_P}{b^2\left[-\frac{b}{a} + \sqrt{\left(\frac{b^2}{a^2} + 3\right)}\right]^2} \tag{2.20}$$

Method 2: Differentiation of moment equation

Equating the total internal moment of the plate to its total external moment,

$$\frac{1}{6}qbx^2 + \frac{1}{8}qb^2(a - 2x) + \frac{1}{12}qb^2 x = M_P b + M_P a \tag{2.21}$$

Differentiating the above equation with respect to x ends up with,

$$x = \frac{b}{2} \tag{2.22}$$

Substituting Eq. (2.21) by Eq. (2.22) will give the limit load,

$$q = \frac{M_P(a+b)}{-\frac{1}{24}b^3 + \frac{1}{8}b^2 a} \tag{2.23}$$

Method 3: Graphical method

If we substitute Eq. (2.21) by $x = \lambda a$, the equation can be represented as,

$$\frac{q}{M_P} = \frac{\frac{2(a+b)}{ab^2}}{\frac{1}{3}\frac{a}{b}\lambda^2 - \frac{\lambda}{3} + \frac{1}{4}} \tag{2.24}$$

For all the above cases,

$$M_P = \frac{1}{4}\sigma_y t^2 \tag{2.25}$$

Let us consider the following parameters for an all edges simply supported plate:

Length of the plate, a = 2000 mm

Width of the plate, b = 800 mm

Thickness of the plate, t = 10 mm

Yield strength of the plate, σ_y = 180 MPa

Plotting $\frac{q}{M_P}$ vs λ from Eq. (2.24),

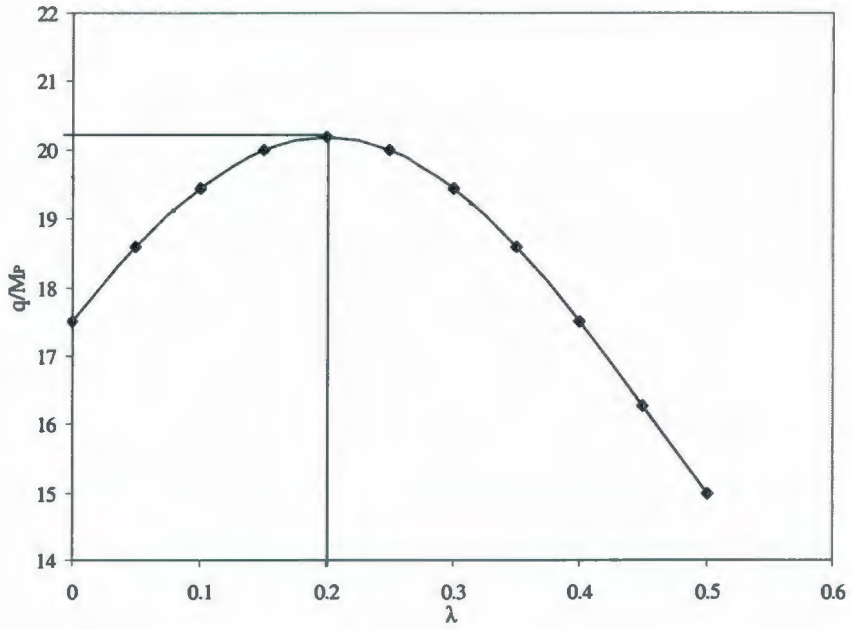

Figure 2.4 Variation of limit load with the location of plastic hinge lines

From Figure 2.4 it can be concluded that the highest $\frac{q}{M_P}$ ratio will render the upper bound limit load in the graphical method of limit load determination.

Table 2.2 shows the limit load results from the above three methods for the parameters mentioned above and comparison of those results with the nonlinear finite element analysis (NFEA).

Table 2.2 Limit load (in kPa) for rectangular plates (thickness 10, 15 and 20 mm)

(a) All edges simply supported

Method 1	Method 2	Method 3	NFEA
88.91	90.87	90.87	94.5
200.06	204.45	204.45	213.3
355.66	363.46	363.46	379.4

(b) All edges fixed

Method 1	Method 2	Method 3	NFEA
177.83	181.73	181.73	203
400.12	408.89	408.89	435.9
711.32	726.92	726.92	717.8

Nonlinear finite element analysis is the elastic plastic solution, therefore for collapsing the structure it has to overcome both elastic energy and plastic energy. On the other hand, these analytical solutions are developed considering the structure as rigid-plastic. Therefore collapsing the structure is only limited by plastic energy which is less than the combined elastic plus plastic energy. That is why analytical limit load results are lower than that of NFEA. If the elastic modulus of the material is significantly increased while performing NFEA, the plastic solution obtained will be very close to the analytical solutions.

2.4 Stress Classification and Limit Stresses

Once the stress distribution in a structure or component is obtained from linear elastic FEA, the designer must categorize the individual stresses and evaluate them, since not all types of stresses, or their combinations, require the same safety factors in protection against failure.

When a component or structure is subjected to mechanical loading such as pressure, distributed load etc, the yielding will continue until the component breaks, considering its material property as elastic-perfectly-plastic. Stresses caused by such loads are not reduced in magnitude by the deformation they produce and thus they are not self limiting.

When a component or a structure is subjected to thermal expansion load or if the member is subjected to stresses attributable to a discontinuity or incompatibility, those stresses are reduced in magnitude by the deformation they produce and thus they are self limiting.

Moreover there may be stresses developed in the region of local structural discontinuities for example at a notch tip or at thermal gradient. These stresses do not cause any noticeable distortion in the component or structure and are objectionable only as a possible source of fatigue cracks or brittle fracture.

The ASME Boiler and Pressure Vessel Code (2007) provides guidelines for the classification of linear elastic stresses in components and structures into (a) primary, (b)

secondary and (c) peak stress categories. The definition and basic characteristics of these stress categories and their role in practical component design is discussed below:

(a) Primary Stress

Primary stresses are set-up in a mechanical component or structure in order to equilibrate the applied external traction. The basic characteristic of primary stress is that it is not self-limiting. The definition of primary stress that is spelled out in the code (ASME B&PV, 2007) is as follows:

> *Primary stress is any normal stress or a shear stress developed by an imposed loading which is necessary to satisfy the laws of equilibrium of external and internal forces and moments.*

(b) Secondary Stress

Secondary stress is developed in a component or structure in order to satisfy geometric compatibility conditions. Secondary stresses are generally developed in regions of gross structural discontinuities, due to internal and external constraints produced by the mechanical loads, or they are due to differential thermal loads. The basic characteristic of a secondary stress is that it is self-limiting. Local stress concentrations are not considered in secondary stresses. The definition of the secondary stress that is spelled out in the code (ASME B&PV, 2007) is as follows:

> *Secondary stress is a normal stress or a shear stress developed by the constraint of adjacent material or by self-constraint of the structure.*

(c) Peak Stress

Peak stress is the large stress intensity in a structure concentrated on an infinitesimal area. It is the highest stress in a component or structure produced by a notch or thermal gradient. Peak stresses are generally developed in regions of local structural discontinuities. The basic characteristic of peak stress is that it does not cause any noticeable distortion in the component or structure and is eventually redistributed under static loading. The definition of peak stress that is spelled out in the Code (ASME B&PV, 2007) is as follows:

> *Peak stress is that increment of stress which is additive to the primary plus secondary stresses by reason of local discontinuities or local thermal stress including the effects, if any, of stress concentrations.*

2.5 Need for Robust Limit Analysis Techniques

An investigation into the literature of limit analysis reveals that considerable amount of effort has been expended towards the analytical determination of limit load. The bounding methods for determining limit loads are mathematically complicated for complex geometries, loading or boundary conditions. Moreover, the accuracy of the method is affected by the underlying simplifying assumptions.

With the advent of high speed computers and the development of the finite element technique, inelastic finite element analysis has emerged as a versatile tool for carrying out elastic-plastic analysis with no strain hardening. However inelastic finite element analysis

also has some inherent draw backs. In inelastic finite element analysis, better estimates of the limit load are found by successive bisections of the load increment. Since this method always operates at the convergence limit, many steps are required to obtain a good estimate of the limit load. Numerical difficulties can also be encountered when the calculated deformations become large as plastic hinges form. Shear locking (Borrval, 2009) is one of the difficulties that may be encountered. Shear locking is caused by the inability of an element to assume a curved shape under the effect of bending. This artificially introduces a shear stress which causes the element to generate shear deformation instead of bending deformation and results in artificially increased stiffness of the element. Thus, the element becomes "locked" or overly stiff in bending. Another difficulty that may be encountered is volumetric locking (Xia and Zhang, 2009). For a metal in the plastic region, a Poisson's ratio approaching a value of 0.5 needs to be considered. This will result in an infinite value for the bulk modulus. A material having an infinite bulk modulus behaves as an incompressible material. Thus, volumetric deformations are locked. Both effects can be remedied only by a judicious choice of the element type and the mesh size used for the analysis.

Apart from the above, limit load values obtained by nonlinear finite element analysis, although accepted as the most accurate, do incur a higher cost per run. Therefore, a detailed nonlinear analysis may not be a viable alternative in situations where results are needed within a short time frame as discussed in the first chapter. This clearly shows the advantage of developing robust approximate techniques, which are simple, reliable

methods based on linear elastic analysis and are capable of predicting inelastic response with acceptable accuracy.

Robust method in the present context implies an ability to provide acceptable results, together with an economy of computational effort. Robust methods are sometimes the only way of verifying nonlinear analysis results of a complex problem. In a word, robust methods are simple, inexpensive and pragmatic alternatives.

2.6 Closure

The evaluation of lower bound limit load in a single linear elastic analysis and accurate limit load based on EMAP can be considered as robust methods for performing limit load analysis. These methods are simple, rapid, and ensure sufficiently accurate lower bound results. Their applicability is not limited by the extent of the problem complexity.

CHAPTER 3

EVOLUTION OF THE m_α-TANGENT METHOD

3.1 Introduction

Limit load is a quantitative measure of the maximum load carrying capacity of a structure. Limit analysis is concerned with the estimation of the load at which a structure or component will collapse (uncontained plastic flow occurs). Limit analysis is especially attractive as it simplifies in the inelastic analysis by assuming an elastic-perfectly-plastic material model. The limit load multiplier scales the applied loads proportionally to that level where the structure reaches its limit state. The exact limit load multiplier can only be obtained by performing an elastic-plastic limit analysis. Consider a body made of an elastic–perfectly-plastic material that is in equilibrium with the surface traction T_i acting

on the surface S_T. On the surface S_u, the constraint $\dot{u}_i = 0$ is applied as shown in Figure 3.1. It is assumed that the surface traction is applied as proportional loading. When the load mT_i is applied, the body will be in a state of impending plastic deformation. Here, m is the exact limit load multiplier or, in other words, the structural factor against plastic collapse. The limit load of a structure is then evaluated as:

$$T_i\big|_{Limit} = mT_i \tag{3.1}$$

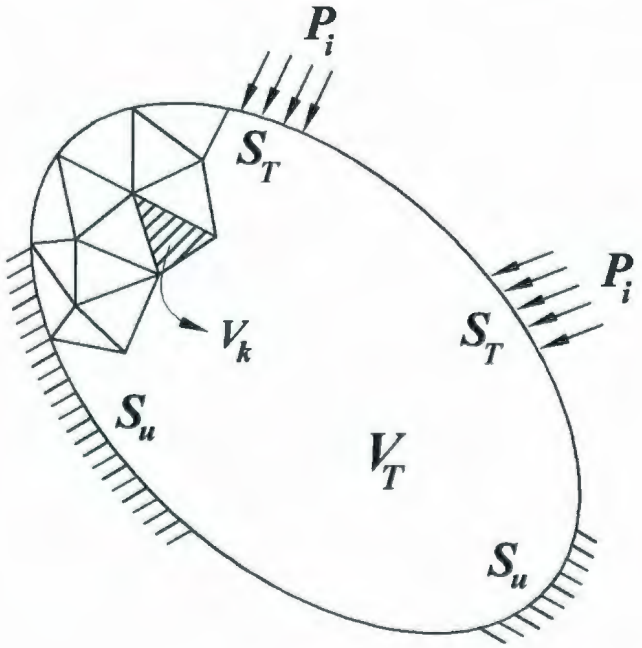

Figure 3.1 Finite element discretization of a body

3.2 Review of Limit Load Multipliers

Several estimates and bounds of the limit load multipliers can be obtained from an elastic analysis. Some of these limit load multipliers are discussed below.

3.2.1 Classical Lower Bound

A lower bound multiplier can be directly obtained by applying the lower-bound theorem of plasticity (Mendelson, 1968). A lower bound multiplier is obtained by assuming the stress distribution throughout the structure to be in equilibrium with the external loads while at the same time not violates the yield criterion. In other words, a given structure will withstand the applied load by rearranging internal stresses to the best possible advantage. The highest lower bound limit load would correspond to the exact limit load. Lower bound limit loads are appropriate for assuring safe component designs.

If σ_y is the yield strength of the elastic-perfectly-plastic material and σ_{max} is the maximum stress value in the total structure, then the classical lower bound limit load multiplier,

$$m_L = \frac{\sigma_y}{\sigma_{max}} \tag{3.2}$$

If P is the arbitrary applied load to the component and P_L is the lower bound limit load then,

$$P_L = m_L P \tag{3.3}$$

The statically admissible stress distribution can be constructed by "inspection", or by using a linear elastic solution. When a finite element analysis is performed, the stress distribution inside each element is approximated. Therefore the lower bound limit load multiplier obtained from linear elastic FEA is a mesh-dependent estimate that is expected to converge to the exact value if the mesh is refined successfully. Moreover, the

maximum equivalent stress (σ_{max}) of the structure has to be evaluated assuring that the existing stress distribution in the structure is primary. The presence of peak stress may cause the σ_{max} value excessively higher which leads to a very conservative lower bound multiplier.

3.2.2 Classical Upper Bound

The upper bound multiplier, m_U , can be obtained from the upper-bound theorem of plasticity (Mendelson, 1968). Assume an estimate of the limit load of a component or a structure is made by equating the internal rate of dissipation of energy to the rate of external work for any strain and displacement field which corresponds to a postulated mechanism of deformation that is kinematically admissible. The limit load estimate will be either high or correct. The equation that determines the upper bound multiplier m_U is,

$$m_U = \frac{\int_{V_T} \sigma_y \, \varepsilon_{eq} \, dV}{\int_{V_T} \sigma_{eq} \, \varepsilon_{eq} \, dV} \Leftrightarrow \frac{\sigma_y \sum_{k=1}^{N} \left(\varepsilon_{eq} \, \Delta V\right)_k}{\sum_{k=1}^{N} \left(\sigma_{eq} \, \varepsilon_{eq} \, \Delta V\right)_k} \tag{3.4}$$

Here ε_{eq} is the equivalent strain.

3.2.3 Upper Bound Multiplier m^0

In classical limit analysis, the statically admissible stress field (equilibrium set) cannot lie outside the yield surface, and the stress associated with a kinematically admissible strain rate field in calculating the plastic dissipation should lie on the yield surface. Mura *et al.* (1965) proposed an approach to eliminate such a requirement, and replaced them with the

concept of "integral mean of yield" in the context of a variational formulation. Based on the "integral mean of yield" (Mura *et al.*, 1965) criterion, the upper bound multiplier m^0 can be obtained as (Seshadri and Mangalaramanan, 1997)

$$m_1^{\,0} = \frac{\sigma_y \sqrt{V_T}}{\sqrt{\int_{V_T} (\sigma_{eq})^2 dV}} \Leftrightarrow \frac{\sigma_y \sqrt{V_T}}{\sqrt{\sum_{k=1}^{N} \left(\sigma_{eq}{}^2 \Delta V\right)_k}} \tag{3.5}$$

Eq. (3.5) implies that the calculation of $m_1^{\,0}$ is based on the total volume V_T by assuming that the flow parameter is constant throughout the structure. The detailed derivation of the upper bound multiplier is given in the Appendix A for a suitable numerical application.

If plastic flow occurs over a localized region of the structure, $m_1^{\,0}$ will be significantly overestimated. To overcome this problem, Pan and Seshadri (2002) have proposed an improved formulation for evaluating m^0 (named as $m_2^{\,0}$). It is based on the idea that m^0 is a distributed parameter that characterizes the degree of collapse at a given location, and can be readily evaluated (derivation is given in Appendix B for a suitable numerical application).

$$m_2^0 = \sigma_y \sqrt{\frac{\int_{V_T} \frac{\varepsilon_{eq}}{\sigma_{eq}} dV}{\int_{V_T} \sigma_{eq} \varepsilon_{eq}\, dV}} \Leftrightarrow \sigma_y \sqrt{\frac{\sum_{k=1}^{N} \left(\frac{\varepsilon_{eq}}{\sigma_{eq}} \Delta V\right)_k}{\sum_{k=1}^{N} \left(\sigma_{eq} \varepsilon_{eq} \Delta V\right)_k}} \tag{3.6}$$

This m_2^0 multiplier is either larger than or equal to the classical upper bound multiplier m_U. It should be noted that for the first linear elastic analysis there is no

difference between m_1^0 and m_2^0. Therefore for a single linear elastic analysis, it is simply denoted as m^0. Proof of the upper boundedness of m^0 has been presented by Reinhardt and Seshadri (2003).

3.2.4 Extended Lower Bound Multiplier

The lower bound multiplier (m') derived from extended variational principle, is the extended lower bound multiplier (Mura and Lee, 1963 and Mura and Rimawi, 1965). The expression of m' by normalizing with the exact multiplier m (usually unknown) can be represented as,

$$R' = \frac{2R^0}{1+\zeta^2} \tag{3.7}$$

Here $R' = \frac{m'}{m}$, $R^0 = \frac{m^0}{m}$ and $\zeta = \frac{m^0}{m_L}$

The extended lower bound limit load multiplier (m') is shown to be less than that obtained from the classical lower bound theorem which is shown in Figure 7.1.

3.3 Evolution of the m_α-Tangent Method

The m_α-Tangent Method was proposed by Seshadri and Hossain (2009) and the multiplier obtained from the method (the m_α^T-multiplier) was applied to mechanical components and structures. The m_α^T-multiplier was further extended for the components

having significant amount peak stress. The detailed evolution of the m_α-tangent method is discussed below.

3.3.1 The Constraint Map

Primary, secondary and peak stresses are developed in mechanical components and structures when they are subjected to mechanical and thermal loading. Figure 3.2 shows the $\frac{m^0}{m}$ vs $\frac{m^0}{m_L}$ trajectory plot in the context of the elastic modulus adjustment procedure (EMAP), illustrating a progressive loss of constraint from an initial elastic state to a plastic collapse state.

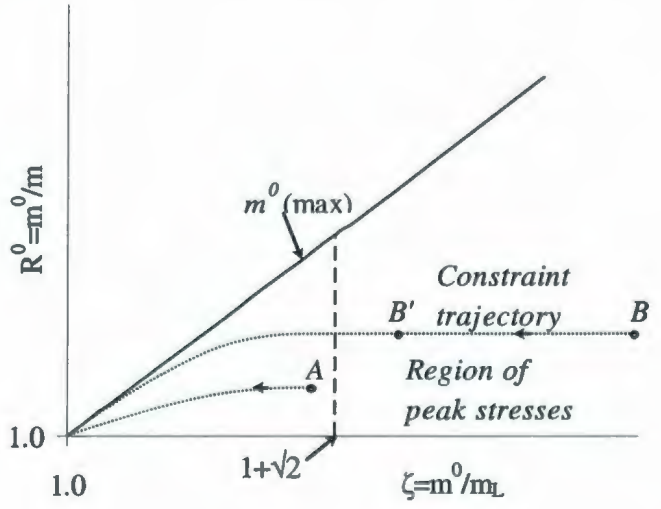

Figure 3.2 The constraint map (Adibi-Asl and Seshadri, 2007)

The ratio $\frac{m^0}{m_L}$ represents a combination of primary, secondary and peak stresses. At the origin, the stresses are purely primary (limit state), and therefore load-controlled. The

ratio $\frac{m^0}{m_L} > 1$ indicates the existence of secondary and peak stresses, along with primary stresses.

The ratio $\frac{m^0}{m}$ represents a combination of primary and secondary stresses for which $\frac{m^0}{m} > 1$. A trajectory (as shown in Figure 3.2) that proceeds toward the origin with a continuous reduction in the magnitudes of $\frac{m^0}{m_L}$ and $\frac{m^0}{m}$, points to a corresponding reduction in the degree of "statical indeterminacy." In this context, the plot of $\frac{m^0}{m_L}$ versus $\frac{m^0}{m}$ is a "constraint map" in which m^0, m_L and m are essentially "scalar measures." Points A and B in Figure 3.2 represent the state of indeterminacy of a given component or a structure. According to Figure 3.2, if we proceed from B to B', by suitably adjusting the elastic modulus of the elements, it eliminates the kinematically inactive volume by scaling up their stress levels, and blunts the peak stress through redistribution. On the other hand, point A in Figure 3.2 corresponds to the components having a negligible amount of kinematically inactive volume and peak stresses.

3.3.2 The m_α –multiplier

The m_α-multiplier expression was developed by Seshadri and Mangalaramanan (1997) using variational calculus methods. The method has explicit dependency on the upper bound multiplier, m^0 and the classical lower bound multiplier, m_L. The upper bound

multiplier, m^0 depends on the entire stress distribution in a component or structure whereas m_L depends on the magnitude of maximum stress. Therefore, for components with sharp notches and cracks the value of m^0/m_L will be high due to presence of peak stresses.

By normalizing with the exact multiplier m (usually unknown), the expression of m_α can be represented as,

$$R_\alpha = 2R^0 \frac{2\zeta^2 + \sqrt{\zeta(\zeta-1)^2(1+\sqrt{2}-\zeta)(\zeta-1+\sqrt{2})}}{(\zeta^2+2-\sqrt{5})(\zeta^2+2+\sqrt{5})} \qquad (3.8)$$

Here $R_\alpha = \frac{m_\alpha}{m}$, $R^0 = \frac{m^0}{m}$ and $\zeta = \frac{m^0}{m_L}$

From Eq. (3.8) it is evident that, the m_α-multiplier is real only within the region $1 \le \zeta \le \left(1+\sqrt{2}\right)$ which is shown by the triangle in Figure 3.3. The condition for lower boundedness of m_α was discussed by Reinhardt and Seshadri (2003). In a two-dimensional space the $R_\alpha = 1$ line can be represented by plotting R^0 vs ζ based on Eq. (3.8) as shown in Figure 3.3. Due to normalization, $R_\alpha = 1$ represents the boundary between the upper bound ($R_\alpha > 1$) and lower bound ($R_\alpha < 1$) as shown in Figure 3.3.

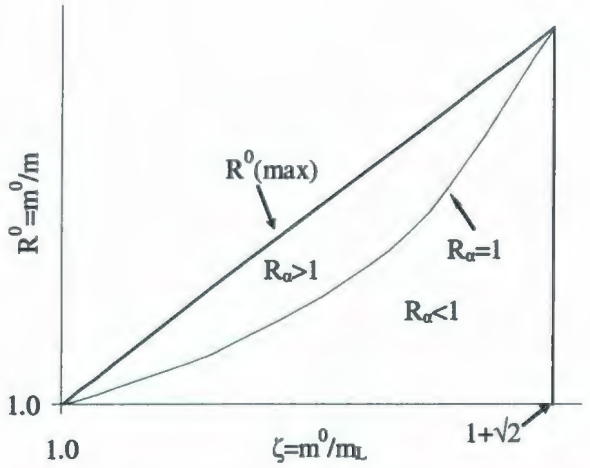

Figure 3.3 Regions of lower and upper bounds of m_α (Reinhardt and Seshadri, 2003)

Now considering $R_\alpha = 1$, Eq. (3.8) becomes,

$$R^0 = \frac{(\zeta^2 + 2 - \sqrt{5})(\zeta^2 + 2 + \sqrt{5})}{4\zeta^2 + 2\sqrt{\zeta(\zeta-1)^2(1+\sqrt{2}-\zeta)(\zeta-1+\sqrt{2})}} \qquad (3.9)$$

3.3.3 The Reference Two-Bar Model

The two-bar model (TBM) (Adibi-Asl and Seshadri, 2007), as shown in Figure 3.4, is the simplest structure in which stress redistribution occurs after the onset of yielding. As such, it serves as a simplified representation of similar redistribution phenomena in any mechanical or ship structure component. The geometry of the TBM can be adapted to best reflect the behaviour of the component. These components or structures are related to the reference two-bar structure by using the "integral mean of yield" criterion. Seshadri and Adibi-Asl (2007) derived the "scaling equations" as follows (Figure 3.4),

$$\frac{m^0{}_{comp}}{m_{L,comp}} = \frac{m^0{}_{bar}}{m_{L,bar}} \left(= \frac{1}{\sqrt{\lambda}} \right) \tag{3.10}$$

$$\frac{m^0{}_{comp}}{m_{comp}} = \frac{m^0{}_{bar}}{m_{bar}} \left(= \frac{1+\lambda}{2\sqrt{\lambda}} \right) \tag{3.11}$$

where $\lambda = \frac{L_1}{L_2} = \frac{\sigma_2}{\sigma_1}$

L_1 and L_2 are the lengths of the bars, and σ_1 and σ_2 are the respective stresses. Once $m^0{}_{comp}$ and $m_{L,comp}$ are determined on the basis of linear elastic FEA, the value of the stiffness ratio (λ) of the two bars can be determined by using Eq. (3.10) which represents the stress distribution in the actual component. Based on this value for λ, an estimate of m_{comp} can be obtained using Eq. (3.11) which assumes that the ratios of $\frac{m^0}{m}$ are the same for the actual component and the reference two-bar mechanism. It should be noted that, $m_{bar} = \frac{2\sigma_y}{\sigma_1 + \sigma_2}$, where σ_1 corresponds to the maximum equivalent stress $(\sigma_e)_{max}$. Therefore the ratio $\frac{m^0{}_{bar}}{m_{bar}}$ represents a combination of primary, secondary and peak stresses along the TBM trajectory.

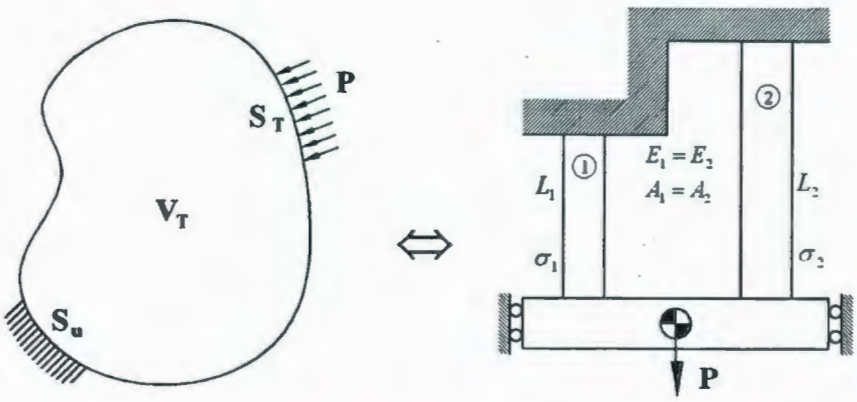

Multidimensional mechanical component Reference Two-Bar Structure

Figure 3.4 Reference two-bar structure (Adibi-Asl and Seshadri, 2007)

For the reference two bar model, Eqs. (3.10) and Eqs. (3.11) can be combined together and can be expressed as

$$R^0 = \frac{m^0}{m} = \frac{1+\zeta^2}{2\zeta} \tag{3.12}$$

Using Eq. (3.12), the entire TBM trajectory can be plotted by considering ζ as a free parameter, as shown in Figure 3.5.

3.3.4 The m_α -Tangent Construction

Eq. (3.8) describes R_α as a function of two variables, R^0 and ζ. The domain of possible values of R_α can be divided as follows, (see Figure 3.5):

1. When $m \to m_L$, the domain of statically admissible m^0 is bounded by the 45-deg (R^0 (max)) line and the positive x-axis. Moreover the $m = m_L$ line is the tangent to the $m = m'$ curve at the limit state as shown in Figure 7.1 (proof is shown in Appendix C).

2. When $m \to m^0$, the domain of statically admissible m^0 is represented by the line $m = m^0$ (positive x-axis). Moreover the $m = m^0$ line is tangent to the TBM trajectory at the limit state as shown in Figure 7.1 (proof is shown in Appendix C).

3. The exact solution (m) locus would lie somewhere between the positive x-axis and the 45-deg line (R^0 (max)).

4. When ζ greater than $1+\sqrt{2}$, R_α becomes undefined. This boundary is indicated as a dashed line in Figure 3.5.

5. The tangent to the R_α=1 curve at the limit state ($m_L = m^0 = m$) will locate the m_α-tangent, which can then be used to estimate the multiplier m provided the reference volume is accounted for.

In order to obtain the slope of the tangent line for the R_α=1 curve at any ζ location, differentiate Eq. (3.9) with respect to ζ. The slope of the tangent line ($R_\alpha^{\,T} = 1$) at the limit state ($m^0 = m_L = m_\alpha = m$) can be obtained as,

$$\left(\frac{dR^0}{d\zeta}\right)_{\zeta=1} = 1 - \frac{1}{\sqrt{2}} \tag{3.13}$$

The equation corresponding to the $R_\alpha^{\,T} = 1$ line can be obtained as,

$$R^0 = 1 + (\zeta - 1)\left(1 - \frac{1}{\sqrt{2}}\right) \tag{3.14}$$

R^0 vs ζ plot based on Eq. (3.14) is represented as the $R_\alpha^{\,T} = 1$ line in Figure 3.5.

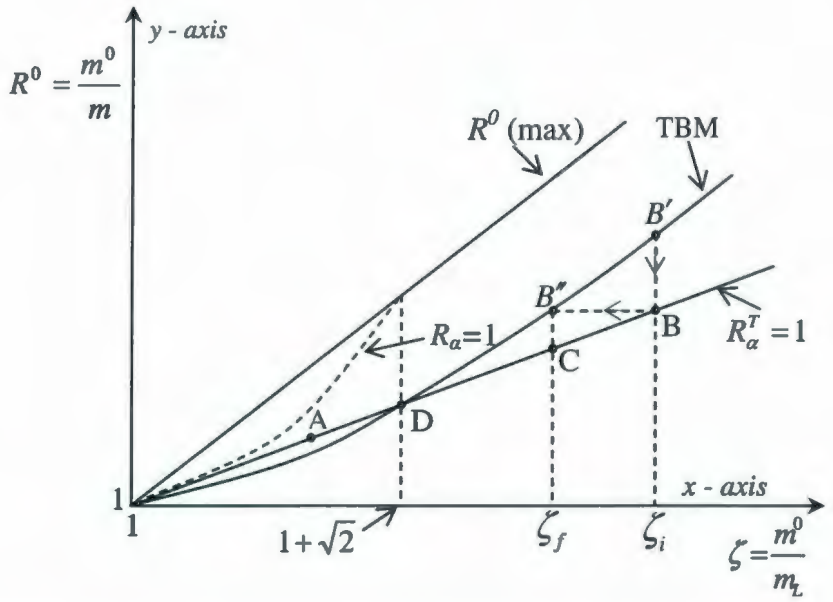

Figure 3.5 The m_α-Tangent construction plot (Seshadri and Hossain, 2009)

The exact limit load multiplier (m) for most practical components and structures is not known a priori. For the m_α-tangent method, R^0 can be defined by making use of the tangent ($R_\alpha^T = 1$ line in Figure 3.5) for any value of ζ. Both R^0 and ζ are greater than one, except at the limit state for which $R^0 = \zeta = 1$.

3.3.5 Characteristics of the m_α-Tangent

With respect to the constraint map, the $R_\alpha^T = 1$ line can be identified, as shown in Figure 3.5. This line is seen to be tangential to the $R_\alpha = 1$ curve at the origin ($R^0 = \zeta = 1$). Furthermore the m_α-Tangent has a relationship to the TBM trajectory as shown in Figure 3.5. Point D (Figure 3.5) can be determined by finding the intersection of the $R_\alpha^T = 1$ line and the TBM trajectory, i.e.,

$$R^0 = 1 + (\zeta - 1)\left(1 - \frac{1}{\sqrt{2}}\right) = \frac{1+\zeta^2}{2\zeta} \tag{3.15}$$

The intersection points work out to be $\zeta = 1$ and $1+\sqrt{2}$. Therefore the TBM trajectory and the m_α-Tangent are very close to each other within the region where m_α is defined. Outside that region, these two trajectories diverge from each other. This divergence can be explained in the light of the fact that the $R_\alpha^T = 1$ line represents a combination of primary and secondary stresses that exist in the components or structures, while the TBM trajectory represents the combination of primary, secondary and peak stresses. Therefore, at point D the peak stresses are negligible (theoretically equal to zero).

3.3.6 Blunting of Peak Stresses

Secondary and peak stresses are set up by redundant kinematic constraints (or static indeterminacy) in a component. ASME Boiler and pressure Vessel codes (ASME 2007) explicitly recognize these stresses and the related constraint effects. Figure 3.6 shows the stress distribution in the ligament adjacent to the notch tip, where the *x*-axis represents the distance ahead of the notch tip, and the y-axis is the equivalent stress. As can be seen from the figure, the magnitude of the equivalent peak stress (σ_F) at the notch tip is considerably high; however, it is assumed that the peak stresses are very localized and that the following expression is valid (Adibi-Asl and Seshadri, 2007).

$$\int_A \sigma_F \, dA = 0 \tag{3.16}$$

where A is the representative area on which σ_F acts.

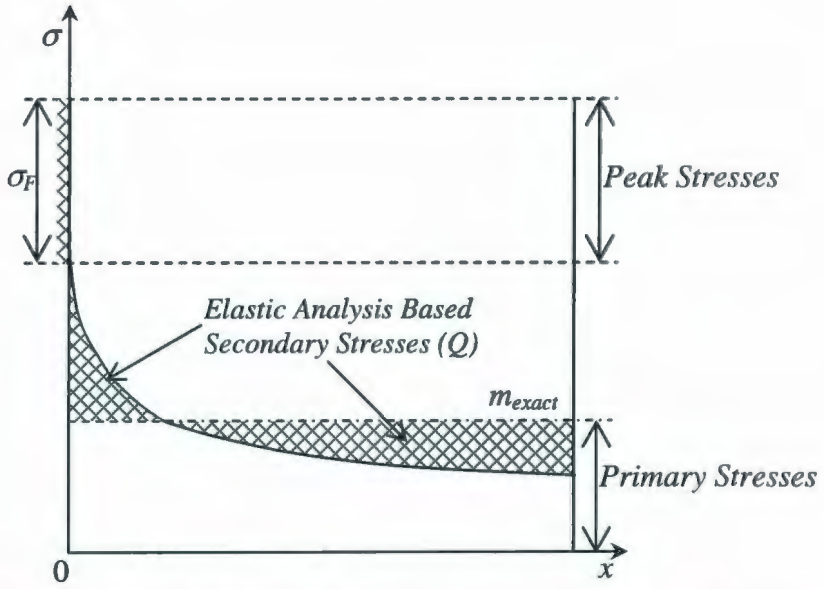

Figure 3.6 Stress distribution ahead of notch tip (Seshadri and Hossain, 2009)

A trajectory in the constraint map that is traversed toward the origin represents, first a blunting of the peak stress, and then the relaxation of secondary stress, until finally, only primary stresses remain.

3.4 The $m_\alpha{}^T$-Multiplier

Once the $R_\alpha^T = 1$ line is identified, the m_α^T value can be readily estimated by Eq. (3.14) as follows:

$$m_\alpha{}^T = \frac{m^0}{1+\left(1-\frac{1}{\sqrt{2}}\right)(\zeta_i - 1)} \tag{3.17}$$

Where $\zeta_i = m^0 / m_L$. The value of m^0 and ζ_i can be determined from statically admissible distributions obtained from linear elastic FEA. Here 'i' is the linear elastic iteration number.

Seshadri and Adibi-Asl (2007) have shown that the two-bar model (TBM) is the simplest structure in which stress redistribution occurs after the onset of yielding. As such, it serves as a simplified representation of similar redistribution phenomena in any mechanical or ship structure component. The geometry of the TBM can be adapted to best reflect the behavior of the component. Utilizing the concept of a two bar model in conjunction with the m_α-tangent construction (Figure 3.5), Seshadri and Hossain (2009) categorized the components into the following two classes on the basis of single linear elastic analysis.

3.4.1 The $m_\alpha{}^T$ Multiplier for Components Having $\zeta_{i=1} \leq 1+\sqrt{2}$

For well-designed components and structures, with smooth geometric transitions, the peak stress effect is negligible and the total volume of the component or structure participates in the plastic action. For these structures, ζ_i lies in between $1 \leq \zeta_i \leq 1+\sqrt{2}$ and $\zeta_i = \dfrac{m^0}{m_L}$ is directly used in Eq. (3.17) in order to evaluate the $m_\alpha{}^T$ Multiplier.

3.4.2 The $m_\alpha{}^T$ Multiplier for Components Having $\zeta_{i=1} > 1+\sqrt{2}$

This case applies to components that develop flaws or cracks in service, or to components with sharp notches. Also, components having some sort of discontinuity or concentrated load over a certain region are in this category. These components may possess significant amounts of peak stress or kinematically inactive volume or a combination of both.

Seshadri and Hossain (2009) extended the $m_\alpha^{\ T}$-multiplier for components having a significant amount peak stress as explained below.

Peak stress correction is done by constructing a horizontal line from point B to B'' signifying an invariant m^0 (blunting of peak stresses) as shown in Figure 3.5. Designate the value of m^0/m_L at B'' as ζ_f, which can be obtained by solving the following equation:

$$\frac{m_i^0}{m} = 1 + (\zeta_i - 1)\left(1 - \frac{1}{\sqrt{2}}\right) = \frac{1 + \zeta_f^{\ 2}}{2\zeta_f} \tag{3.18}$$

The roots of Eq. (3.18) are

$$\zeta_f = (1 + 0.2929\,(\zeta_i - 1)) \pm \sqrt{(1 + 0.2929\,(\zeta_i - 1))^2 - 1} \tag{3.19}$$

Using m^0 and ζ_f, the $m_\alpha^{\ T}$-multiplier expression can be evaluated as

$$m_\alpha^{\ T} = \frac{m^0}{1 + \left(1 - \frac{1}{\sqrt{2}}\right)(\zeta_f - 1)} \tag{3.20}$$

Elastic analysis guarantees a statically admissible stress state and a kinematically admissible strain state. Therefore, unlike classical methods in plasticity, the collapse mechanism is not explicitly required in advance because of an implied statically admissible stress field and a kinematically admissible strain field.

3.5 Discussion

Whenever plastic action occurs over a localized region of the mechanical component or structure it may possess significant amounts of peak stress or kinematically inactive

volume or a combination of both. Lack of proper kinematically inactive volume identification may cause the m_α^T-multiplier to be upper bounded. Therefore further extension of the m_α^T-multiplier for components possessing kinematically inactive volume is of significant interest. This extension will be discussed in chapter 4. It should be mentioned here that, the choice of yield strength does not alter the procedure for calculating limit loads. The effect of different yield strength is simply the introduction of a suitable scaling factor.

CHAPTER 4

NOTION OF KINEMATICALLY ACTIVE VOLUME

4.1 Introduction

When plastic flow occurs over a localized region of the mechanical component or structure, the remaining regions do not participate in inelastic action and may remain elastic at the limit state and therefore only a portion of the total volume carries the external loads at the limit state. The volume that actively participates in plastic action is called kinematically active volume or reference volume and the remaining regions are called kinematically inactive volume or dead volume.

4.2 Dependency of Multipliers on Local Plastic Flow

In the reference volume approach, it is assumed that the primary load is carried by a localized region which causes significant reduction in load carrying capacity of the total component or structure. Therefore, m_1^0 will be significantly overestimated if it is based on the total volume V_T. Furthermore, the corresponding m_L, which is calculated based on a single element that has the maximum equivalent stress in the component, will be underestimated.

Consider a component subjected to arbitrary loading condition, Figure 4.1. The component is divided into two regions: (1) reference volume (V_R), which is kinematically active volume; and (2) the dead volume (V_D), which is kinematically inactive volume. If V_T is the total volume of the mechanical component or structure,

$$V_R + V_D = V_T \qquad (V_R \leq V_T) \tag{4.1}$$

Based on this definition the upper bound multiplier can be expressed as,

$$m_{ref}^0(V_R) = \frac{\sigma_y \sqrt{V_R}}{\sqrt{\int_{V_R} (\sigma_{eq})^2 dV}} \tag{4.2}$$

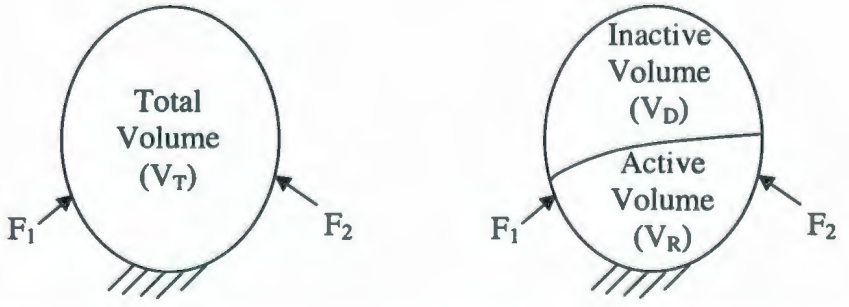

Figure 4.1 Representation of kinematically active and inactive volume

The multiplier m_2^0, Eq. (3.6), can be written in terms of the reference and the dead volume as

$$m_2^0 = \sigma_y \frac{\sqrt{\int_{V_R} (\varepsilon_{eq} / \sigma_{eq}) dV + \int_{V_D} (\varepsilon_{eq} / \sigma_{eq}) dV}}{\sqrt{\int_{V_R} \sigma_{eq} \varepsilon_{eq} dV + \int_{V_D} \sigma_{eq} \varepsilon_{eq} dV}} \tag{4.3}$$

If we assume that the dead zone has no plastic flow occurring, then Eq. (4.3) can be simplified as

$$m_2^0(V_R) = \sigma_y \frac{\sqrt{\int_{V_R} (\varepsilon_{eq} / \sigma_{eq}) dV}}{\sqrt{\int_{V_R} \sigma_{eq} \varepsilon_{eq} dV}} \tag{4.4}$$

4.3 Implicit Reference Volume Correction in EMAP

During local plastic action, plastic flow is confined to a sub-region of the total volume, and the remainder region, being still elastic, will become a zone with zero stress and strain. Hence, the magnitude of the upper bound multiplier (m^0) would depend on the sub-volume, V_R, where

$$V_R = \sum_{k=1}^{\alpha} (\Delta V_k), \text{ and } \alpha < N \tag{4.5}$$

Within which the elements are arranged in the order of

$$(\sigma_{e1}^0)^2 \Delta V_1 > (\sigma_{e2}^0)^2 \Delta V_2 > \ldots\ldots > (\sigma_{en}^0)^2 \Delta V_n \tag{4.6}$$

An iteration variable ζ was introduced by Seshadri and Mangalaramanan (1997) in such a way that infinitesimal changes to the element elastic modulus of the various elements during the second and subsequent linear elastic FEA would induce a corresponding change $\Delta\zeta$. The magnitude of $\Delta\zeta$ would of course depend on the nature of the modulus-adjustments.

Eventually the upper bound multiplier will reduce due to element modulus adjustment in subsequent linear elastic iterations as shown in Figure 4.2 while approaching the final solution. It can be assumed that, in every iteration, m^0 is split into a constant value and a variable portion that vanishes with iterations. Hence,

$$m^0 = m^0_{ref} + \Delta m \tag{4.7}$$

where m^0_{ref} is the constant part and Δm which vanishes after a certain number of linear elastic iterations. It is observed that the vanishing part represents the zone in the component that is not affected by the plastic deformation occurring in the highly stressed zone, and thus, in the state of collapse, its stress level tends towards zero.

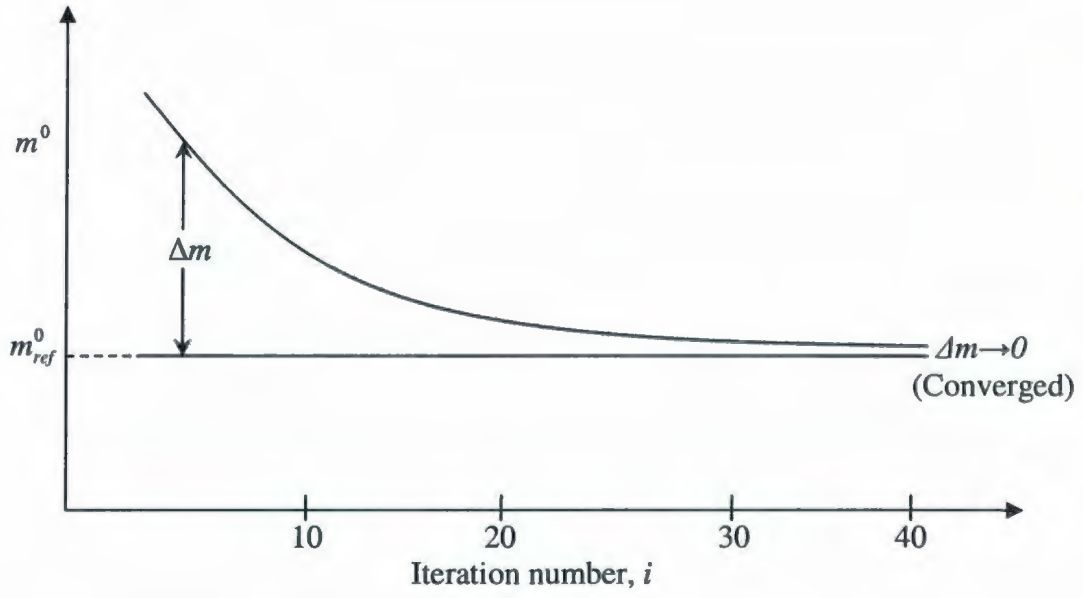

Figure 4.2 Variation of m^0 with Elastic Iterations

Therefore m^0 evaluated on the basis of total volume also decreases in subsequent linear elastic FEA except for the degenerate case, when m^0 would increase with the iteration violating the nesting surface theorem (Calladine and Drucker 1962). Eventually, for some volume V_R, where $\Delta V_1 < V_R \leq V_T$, the multiplier m^0 would be invariant, i.e., $m_i^0 = m_{i+1}^0$. Similarly, lower bound multipliers also converge towards the exact limit load multiplier in subsequent linear elastic iterations due to successive peak stress corrections. The schematic of variation of m^0 and m' with the iterations is shown in Figure 4.3. It is evident from the figure that subsequent linear elastic iterations converge the upper bound and lower bound multipliers towards the exact limit load multiplier. In other words, the reference volume and peak stresses are implicitly corrected in subsequent iterations although a large number of iterations may be anticipated for the convergence of basic

upper bound and lower bound multipliers to the exact limit load multiplier, especially for the three dimensional FEA models.

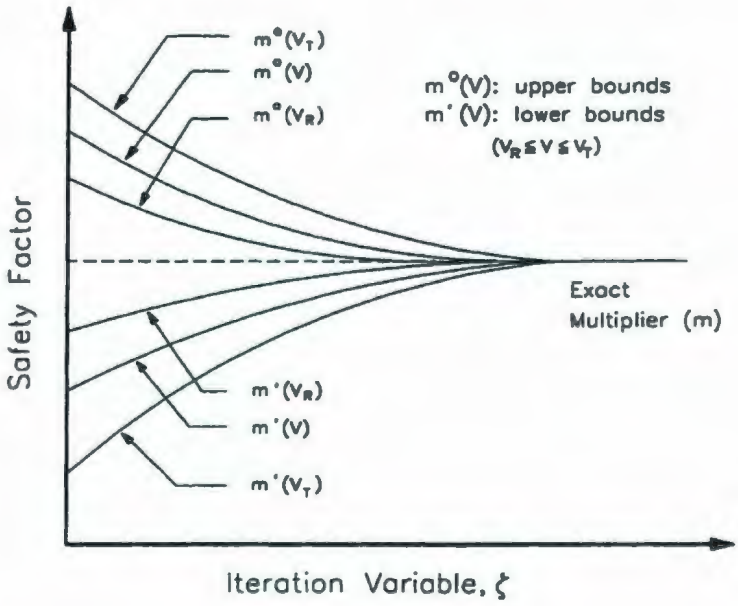

Figure 4.3 Variation of m^0 and m' with Elastic Iterations

4.4 The Proposed Reference Volume Correction

As discussed earlier, the $R_a^T = 1$ line represents a combination of primary and secondary stresses that exist in the components or structures while the TBM trajectory represents the combination of primary, secondary and peak stresses. Therefore once m^0 and m_L are obtained from the linear elastic analysis, points B' and B are identified on the TBM trajectory and the $R_a^T = 1$ line respectively, at the location $\zeta_i = \frac{m^0}{m_L}$, as shown in Figure 3.5. Point B represents the combination of primary and secondary stresses whereas point

B' represents the combination of primary, secondary, and peak stresses. Construct a vertical line from point B' to B signifying the elimination of the inactive volume. The percentage of inactive volume incorporated in m^0 is $\frac{R^0_{B'} - R^0_B}{R^0_{B'}}$. Therefore the kinematically active reference volume based upper bound multiplier can be obtained as,

$$m^0_{ref} = \frac{R^0_B m^0}{R^0_{B'}} \tag{4.8}$$

Substituting $R^0_{B'}$ and R^0_B from TBM trajectory and $R^T_\alpha = 1$ line respectively,

$$m^0_{ref} = \frac{\zeta_i\left(\sqrt{2}\zeta_i\left(\sqrt{2}-1\right)+\sqrt{2}\right)}{1+\zeta_i^{\,2}} m^0 \tag{4.9}$$

4.5 Discussion

Reference volume correction discussed in the above section, can be incorporated to the m_α-tangent method as an additional feature, which ensures lower bound limit load estimation from the m_α-Tangent method based on single linear elastic analysis. Characteristics of the m_α-tangent construction plot due to the inclusion of the additional feature is described in chapter 7 and some numerical examples are also solved on the basis of single linear elastic analysis, using this modification.

CHAPTER 5

MODELLING OF SHIP COMPONENTS

5.1 Introduction

Beams, frames, plates and stiffened panels are the structural building blocks of marine vehicles. The behavior of these components is well understood in the elastic region. However the structural response beyond the elastic range is quite different for various stiffeners and often wrong results are obtained if conventional elastic techniques are used. In recent years there has been a renewed interest in investigating the plastic response of ship structure components. Cui and Mansour (1999) extended the method proposed by Paik and Pedersen (1996) to investigate the effect of parameters like welding distortions and residual stress on the ultimate compressive strength of grillage. Paik at al. (1999) developed the design equations for the ultimate strength of plate subjected to different

types of loading. An analytical method for calculating the ultimate strength of bottom plating of ship structure subject to transverse thrust and lateral pressure was proposed by Fujikubo *et al.* (2005). Moreover the accuracy of existing methods (ANSYS, NLFEA, PULS, ALPS/ULSAP, ALPS/HULL, and IACS CSR) used for the estimation of ultimate strength of marine structures were studied and compared by Paik *et al.* (2008a, 2008b, 2008c). However there are no analytical solutions currently available which can represent the complete plastic response of a stiffened panel considering all possible failure modes. Full scale testing is undoubtedly the best method; however the high cost of fabricating test specimen, complexities involved in accurately measuring responses and the time required to conduct each experiment limits the number of experiments that can be periodically conducted. Finite element analysis (FEA) is a fast and economic alternative compared to full scale test. Therefore FEA based simplified limit load determination techniques (already discussed in earlier chapters) are of great interest to engineers. However these results can only be used after proper validation. Hence the study of non-linear study is also an important issue. Once validated, the simplified technique can then be used to further explore the design space.

5.2 Finite Element Modeling of Ship Structure Components

5.2.1 Fixed End Beam

A fixed end beam (shown in Figure 5.1) with length, L = 508 mm; height, h = 25.4 mm and width, w=25.4 mm is modeled. The modulus of elasticity of the material is 206.85

GPa and yield strength is 206.85 MPa. The beam is subjected to uniformly distributed load of 1 MPa. The model is meshed using PLANE82 elements.

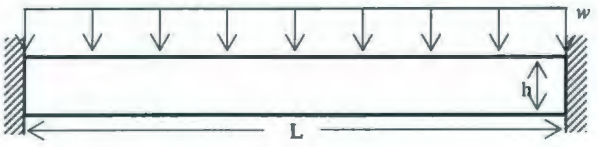

(a) Beam geometry

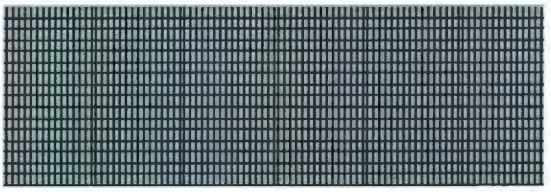

(b) Finite element model segment (plane stress)

Figure 5.1 Fixed end beam

5.2.2 Transverse Ship Frame Subjected to Hydrostatic Pressure

A ship's transverse frame is an integral part of the whole ship structure that acts together to resist various types of environmental loads. Under normal conditions, the transverse frame act to provide transverse strength, to resist raking, to resist lateral hydrostatic pressure due to sea pressure, to resist shear and torsional deflection of the hull and also to stabilize the shell plating and provide in plane shear stiffness. Figure 5.2 shows a transverse ship frame subjected to hydrostatic pressure. Hydrostatic pressure varies linearly from 1.65 MPa at the bottom to 0 MPa at the free surface. The modulus of elasticity of the material is 206.85 GPa and yield strength is 206.85 MPa. The model is meshed using PLANE82 elements.

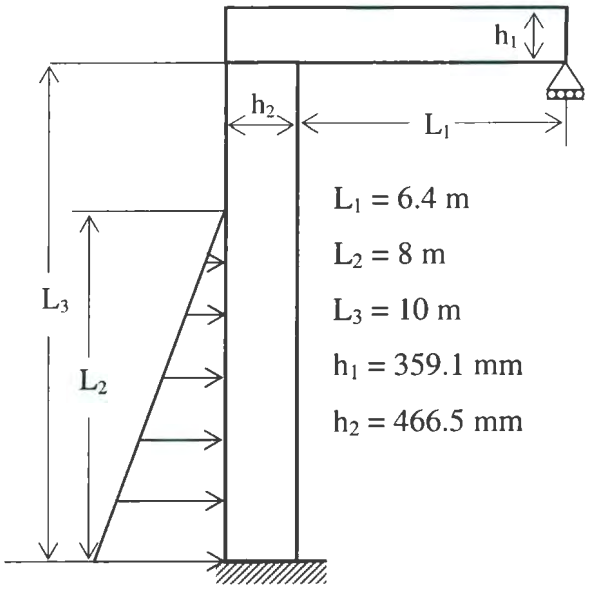

(a) Geometry

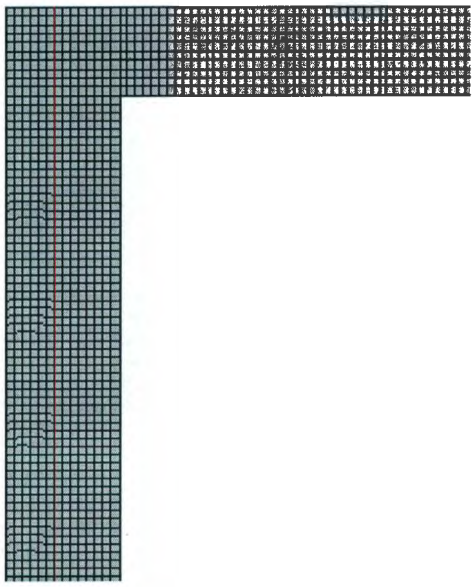

(b) Finite element model segment (plane stress)

Figure 5.2 Transverse ship frame

5.2.3 Rectangular plates under uniform pressure

Plates are one of the most important components of a ship's structure. In the current study, plates of three different thickness and two different boundary conditions have been investigated in order to determine the limit load of the plates. The significance of this part lies on the meshing strategy of ship structure components while applying the simplified limit analysis techniques.

Convergence studies have been performed for this example problem to verify the sensitivity of the $m_\alpha{}^T$-multiplier, with respect to mesh density which is shown in Figure 5.3. From Figure 5.3 it is evident that, in order to improve accuracy of result, it is recommended to use more element divisions along the thickness of any plate subjected under pressure loading. For this example nine element divisions have been chosen per ten millimeters of thickness, which gives results of adequate accuracy and is optimum as well in terms of computation time required for elastic analysis. The variation of $m_\alpha{}^T$-multiplier is mostly due to the variation of m_L which is sensitive to peak stresses. Thus whenever the variation of m_L decreases, the $m_\alpha{}^T$- multiplier becomes invariant with the variation of mesh intensity.

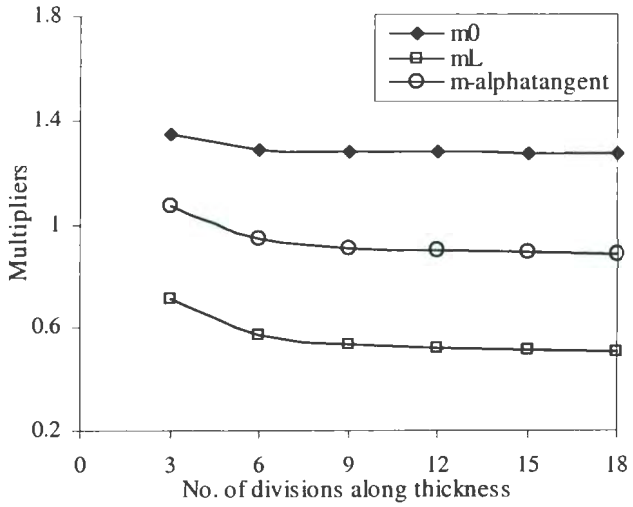

(a) Plate thickness = 10 mm

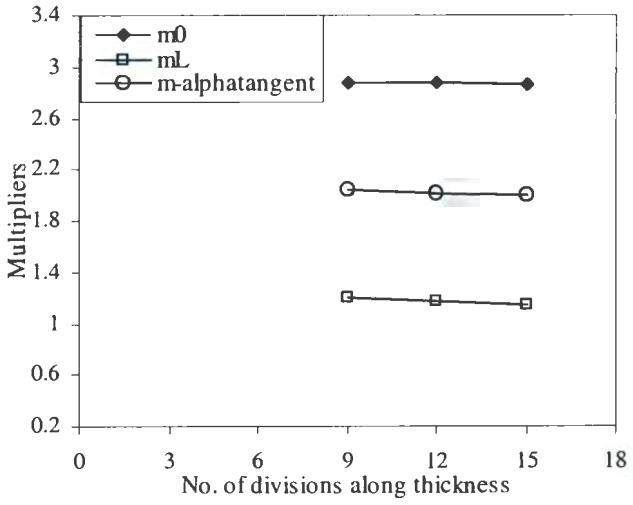

(b) Plate thickness = 15 mm

Figure 5.3 Mesh sensitivity test for simply supported plate (Continued)

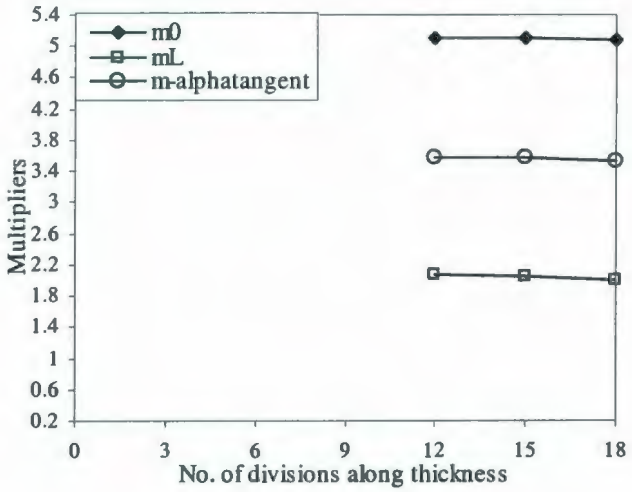

(c) Plate thickness = 20 mm

Figure 5.3 Mesh sensitivity test for simply supported plate

Detailed plate parameters required for FEA of plates are described below:

Plate Dimensions:

Length = 2000 mm

Width = 800 mm

Thickness = 10, 15, 20 mm

Element Type:

Three dimensional twenty nodded element (SOLID95)

Element Divisions:

Along length = 120

Along width = 60

Along thickness = 9, 15 and 18 divisions for 10 mm, 15 mm and 20 mm thickness respectively.

Material Properties:

Modulus of Elasticity, EM = 209 GPa

Poisson Ratio, PR = 0.47

Yield Strength, YM = 180 MPa

Nonlinear Material Model: Elastic perfectly plastic

Boundary Conditions:

All edges simply supported (UX = 0, UY = 0 and BM = 0 at all edges)

All edges fixed (UX = 0, UY = 0, UZ = 0, BM = M at shorter edges)

Transverse Pressure Loading at the Bottom Plane of the Plate:

Whenever the ship structure is submerged under water, the total pressure acting on the bottom of the plate can be expressed as

$$P = \rho g h \qquad (5.1)$$

ρ = 1025 kg/m^3, Density of sea water

g = 9.81 m/s^2, Acceleration due to gravity

h = depth of sea water

For all the problems, the pressure acting on the bottom of the ship is taken as P = 100 kPa, which means that the depth of water is 9.945 m.

5.2.4 Single Stiffened Plate of Ship Structure

A stiffener with the attached shell plate is considered as a representative unit of the entire grillage structure as shown in Figure 5.4. The length of the frame is 2m which is the distance between two transverse members as shown in Figure 5.6(b) and the other dimensions are shown in Figure 5.4(a). The web and the flange of a stiffener are free to move both vertically and horizontally however the shell plate is restricted from moving sideways due to the presence of adjacent structure. Symmetric boundary conditions are applied along the length of the plate to simulate the support provided by the neighboring structure. Shorter ends are fixed to simulate the support provided by the continuing frame and transverse members. Element type, material properties, meshing strategies, and the loading conditions are similar to the plate structure as discussed earlier in section 5.2.3. The finite element meshed model segment is shown in Figure 5.4(c). Figure 5.4(d) gives the von Misses equivalent stress distribution in the structure based on the initial linear elastic analysis, which shows the participation of different portions of the structure in load sharing.

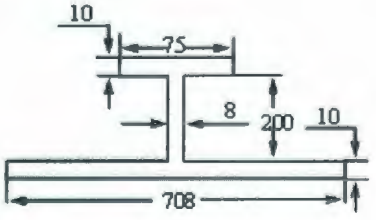

(a) Side view

Figure 5.4 Single stiffened plate of ship structure (Continued)

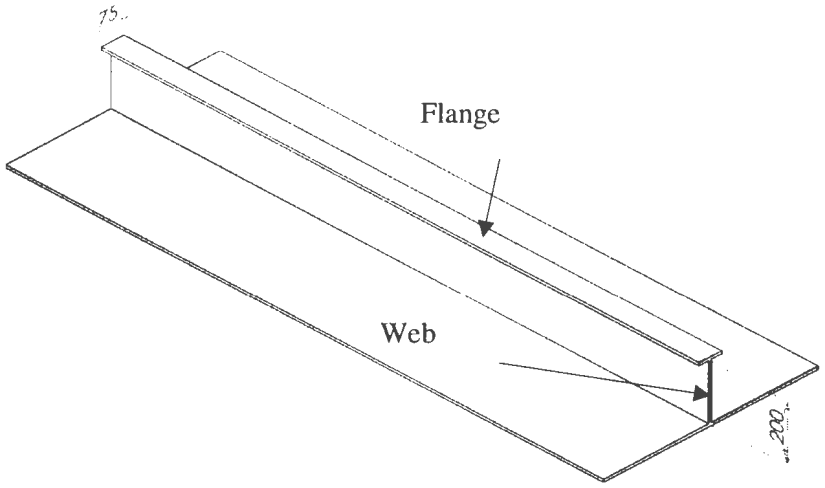

(b) 3D view of single frame

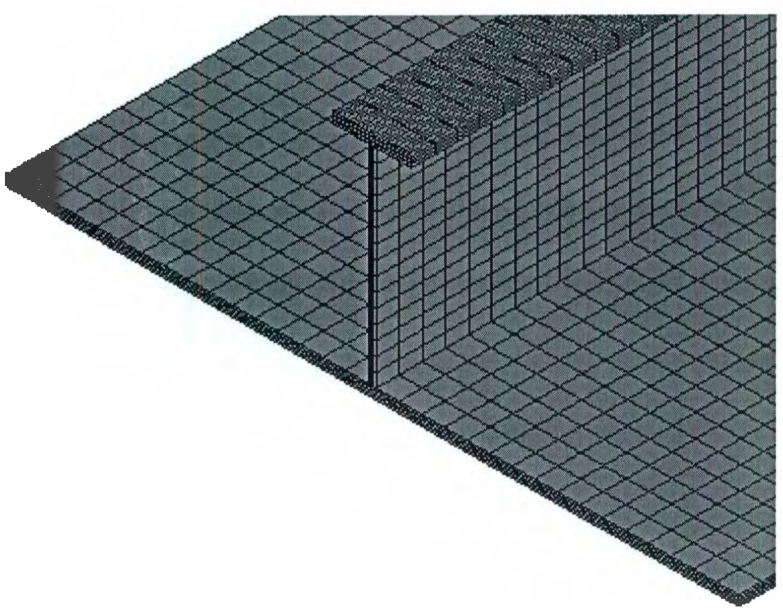

(c) Finite element model segment

Figure 5.4 Single stiffened plate of ship structure (Continued)

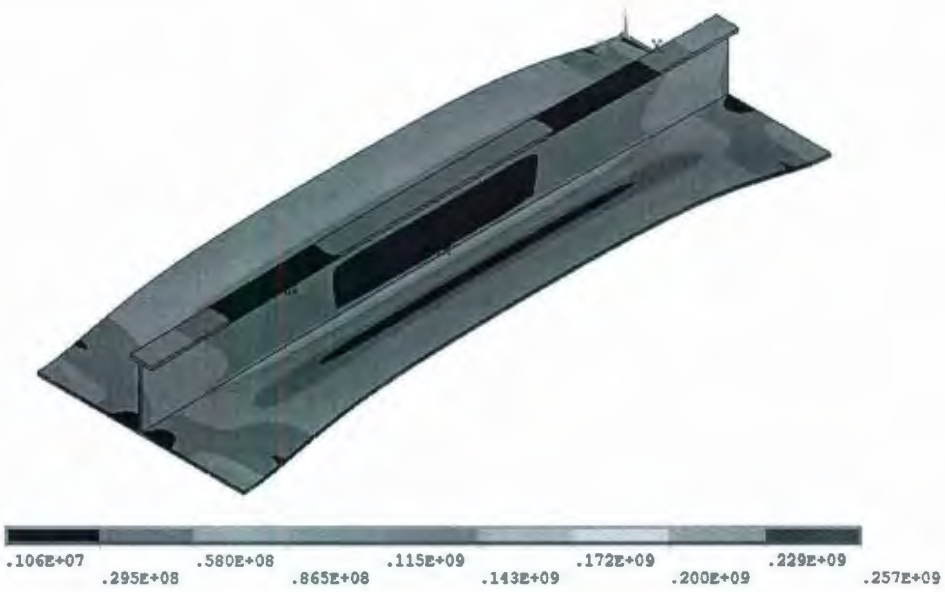

(d) von Misses equivalent elastic stress distribution

Figure 5.4 Single stiffened plate of ship structure (Dimensions in mm)

5.2.5 Small Grillage of Ship Structure

The small grillage is taken as an integrated structure between two heavy transverses as shown in Figure 5.5. The addition of adjacent side structures simulates the actual side boundary conditions for the middle stiffener as shown in Figure 5.5(b). Length of the grillage is 2m which is the distance between two heavy transverse members as shown in Figure 5.6(b) and the other dimensions are shown in Figure 5.5(a).The two longitudinal ends are fixed to represent the boundary condition provided by the heavy transverse members in a ship structure as shown in Figure 5.6(b). Element type, material properties, meshing strategies, and the loading conditions are similar to the plate structure as discussed earlier at section 5.2.3. The finite element meshed model segment is shown in Figure 5.5(c). Figure 5.5(d) is the von Misses equivalent stress distribution in the

structure based on the initial linear elastic analysis, which shows the participation of different portions of the structure in load sharing.

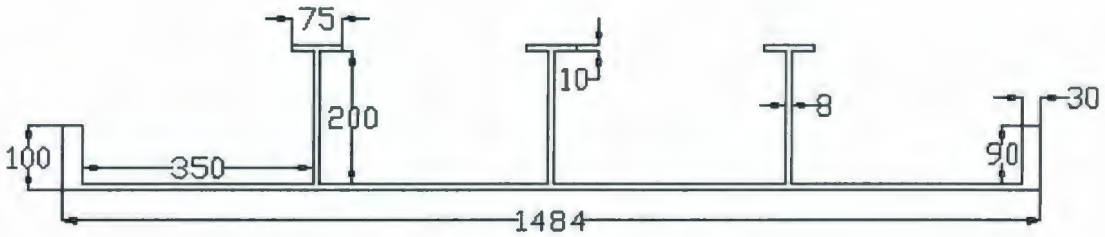

(a) Side view of the small grillage

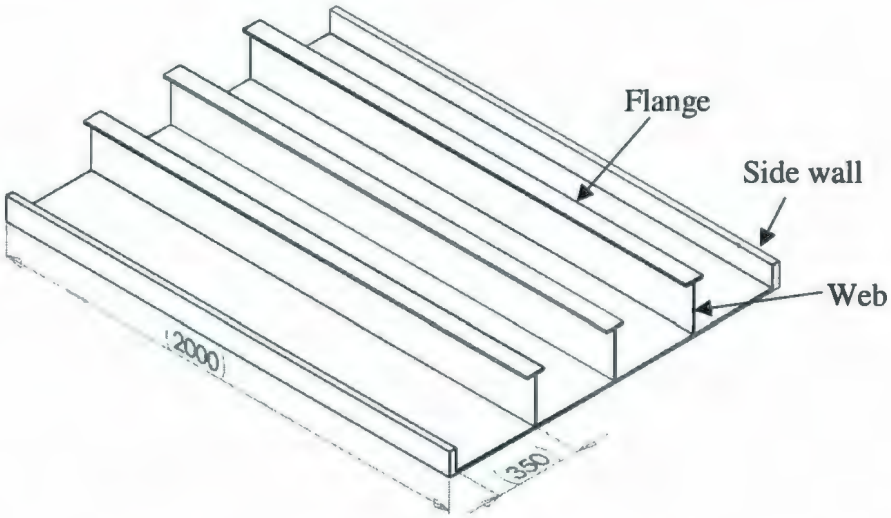

(b) 3D view of small grillage

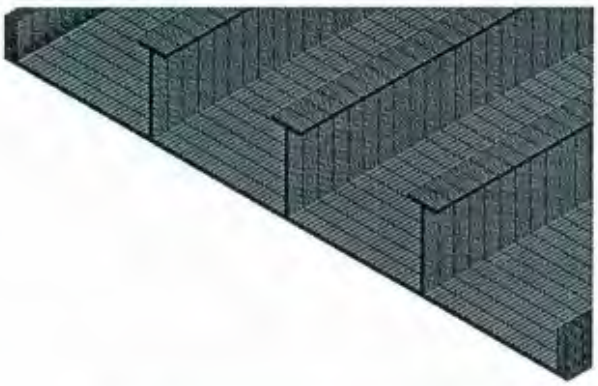

(d) Finite element model segment

Figure 5.5 Small grillage of ship structure (Continued)

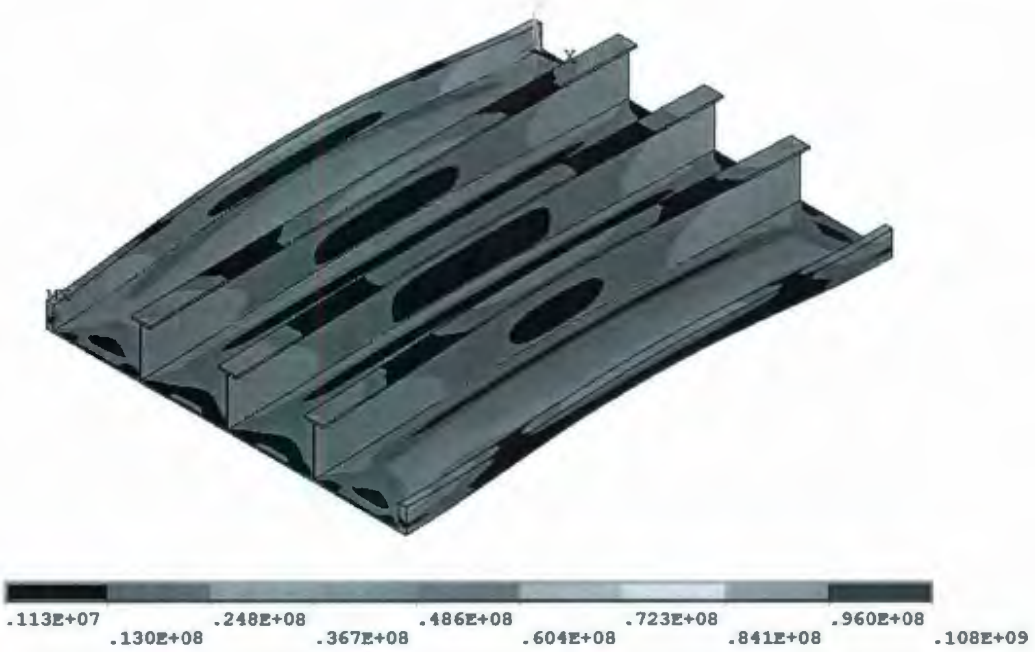

(d) von Misses equivalent elastic stress distribution

Figure 5.5 Small grillage of ship structure (Dimensions in mm)

5.2.6 Large Grillage of Ship Structure

A large grillage consists of three neighbouring frames, each with three frame spans in the longitudinal direction and at each span; a heavy transverse frame is provided which gives the necessary support at that location as shown in Figure 5.6. The longitudinal frame ends and the two transverse frame (stringers) ends of the grillage are fixed. In the finite element modelling half model is used to achieve simplification.

Figure 5.6 represents the general arrangement of the large grillage for the finite element modeling. Figure 5.5(a) shows the side view of the shell plate and longitudinal T stiffeners. Stringers running in the transverse direction are shown in Figure 5.6(a). The stringers are also like T stiffeners but they are heavier and deeper than the longitudinal

stiffeners. The distance between the stringers is 2 m and the other dimensions are shown in Figure 5.6(b).

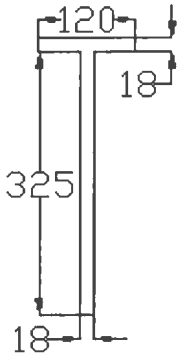

(a) Side view of the transverse member

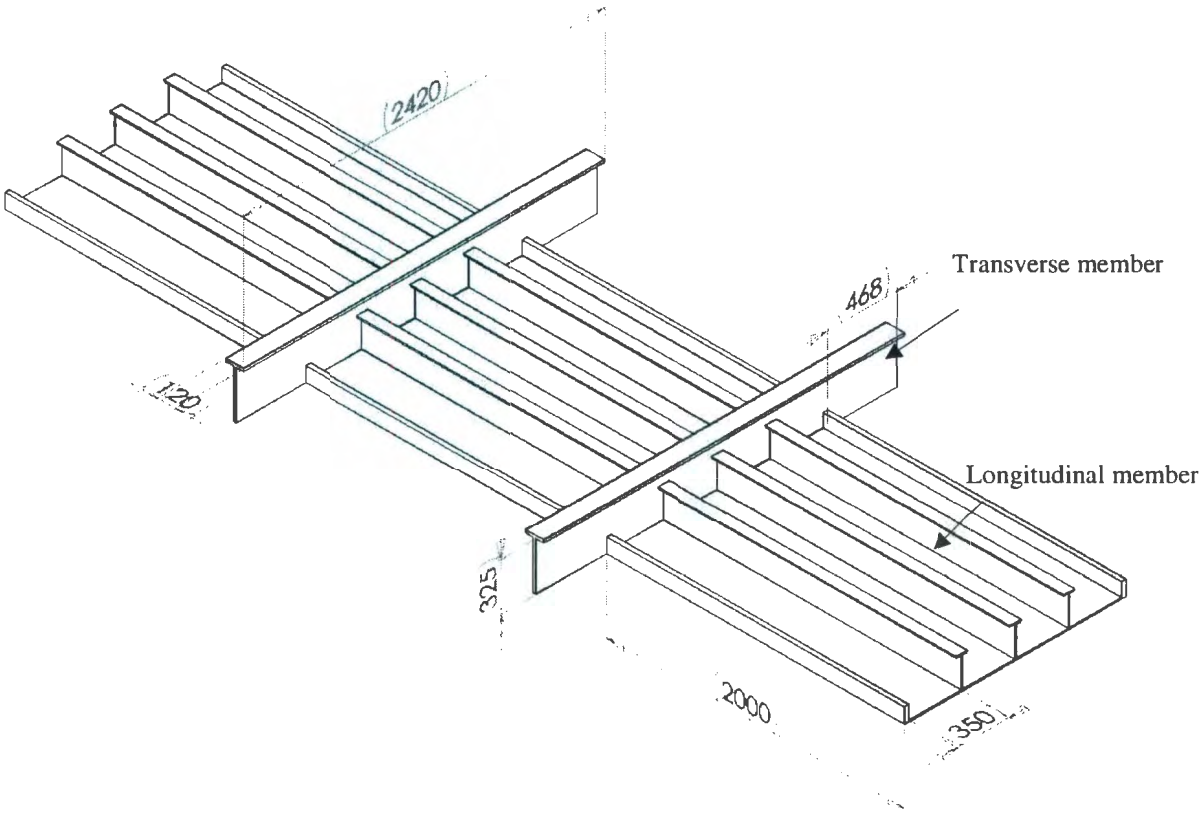

(b) 3D view of large grillage

Figure 5.6 Large grillage of ship structure (Continued)

(c) Finite element model segment

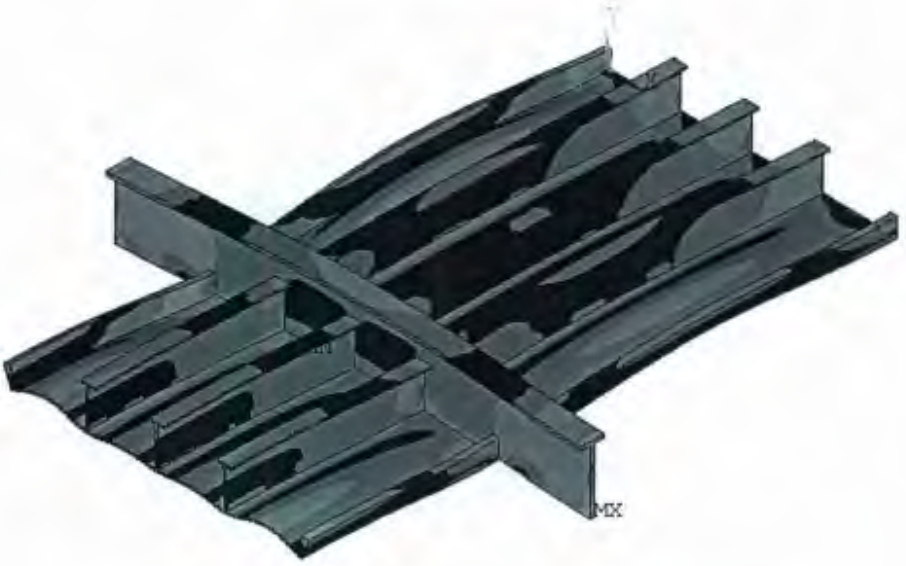

(d) von Misses equivalent elastic stress distribution

Figure 5.6 Large grillage of ship structure (Dimensions in mm)

The model is meshed using SOLID92 elements which is much lighter (in terms of number of nodes) compared to SOLID95. Material properties, meshing strategies, and the loading conditions are similar to the plate structure as discussed earlier at section 5.2.3. The finite

element meshed model segment is shown in Figure 5.6(c). Figure 5.6(d) is the von Misses equivalent stress distribution in the structure based on the initial linear elastic analysis, which shows the participation of different portions of the structure in load sharing.

5.3 Inelastic Finite Element Analysis

In this thesis all the finite element analysis is performed using ANSYS 11.0 (2009). The inelastic finite element analysis is performed using an elastic-perfectly-plastic material model. The load is incremented in steps from the applied load in order to reach the limit state and a solution for each load step is found successively. Within each load step, a large number of sub-steps are set in order to ensure the gradual increase of load applied in that step. The default iterative scheme of Newton-Raphson is used for solving simultaneous non-linear equations. Solution enhancement features like bisection (to decide whether or not to reduce the present time step) and automatic load stepping (to estimate the next time step size) are also used as permitted by the selected iterative scheme. All the methods suggested in this thesis follow small deflection theories. Therefore nonlinear geometry options are not been contemplated in nonlinear analysis. The basic steps of the inelastic finite element analysis using ANSYS are shown in Figure 5.7.

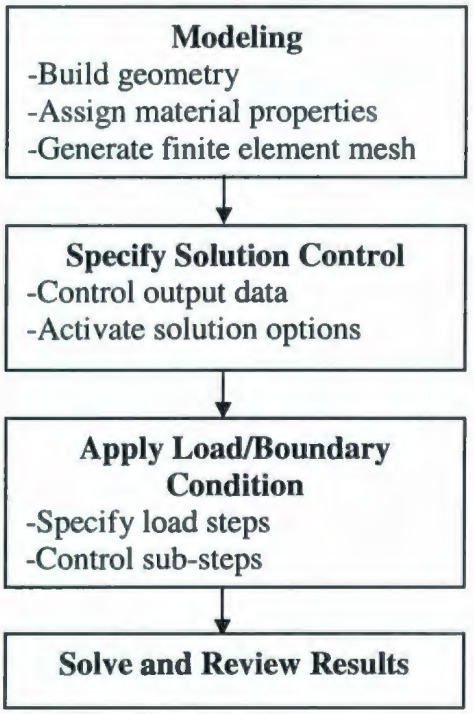

Figure 5.7 Flowchart of inelastic analysis

5.4 Conclusion

A variety of ship structure components have been modeled and each model has been analyzed on the basis of the single linear elastic analysis, iterative linear elastic analysis and the inelastic finite element analysis. Both two dimensional (plane stress problems), and three dimensional models are analyzed and different types of elements have been used for modeling, which ensures the applicability of the proposed simplified methods for any types of material property, geometric property and element type.

For proper comparison, the geometric model, material model, boundary conditions, and applied loading conditions of a particular ship structure component has to be maintained

exactly same while performing the linear elastic analysis and inelastic finite element analysis. In order to ensure it, at first the finite element model of a particular ship component is generated with all its properties (material property, geometric property etc.), boundary conditions, and applied loading conditions. Later the analysis features (elastic analysis and inelastic analysis) are added separately. Mesh sensitivity test of the model for the inelastic FEA is found as important as that of linear elastic FEA. Therefore multiple inelastic analyses for a single model is also performed in order to achieve mesh convergence.

CHAPTER 6

EMAP BASED LIMIT ANALYSIS

6.1 Introduction

The main goal for any FEA based limit analysis is to obtain the limit state stress field. In elastic-plastic analysis, the yield strength is fixed, and the load is increased until lack of convergence indicates that equilibrium cannot be satisfied. Instead of increasing the load, the yield strength of the model can also be reduced at constant load until the collapse occurs, and then loads and stresses are scaled back up to the actual yield stress. EMAP follows such an approach and establishes an inelastic-like stress field by modifying the local elastic modulus in order to obtain the necessary stress redistribution. Numerous sets of statically and kinematically admissible distributions can be generated in this manner, which enable calculation of both lower and upper bound limit load multipliers.

6.2 Mathematical Formulations for EMAP

An arbitrary load set (P) with the original elastic modulus (E_0) is applied in the first iteration of an elastic FEA. Subsequently, the elastic modulus of each element is modified in each successive iteration in the following manner:

$$E^{i+1} = \left(\frac{\sigma^i_{ref}}{\sigma^i_{eq}} \right)^q E^i \tag{6.1}$$

where q is the elastic modulus adjustment parameter, σ^i_{ref} is a reference stress, σ_{eq} is the equivalent stress and the superscript "i" is the iteration number (i=1 for the initial elastic analysis). Impact of different q values on the consistency of limit load multiplier variation with iterations and their convergence rate were reported by Adibi-Asl *et al.* (2006). It was reported that, smaller modulus adjustment parameter assures consistent multiplier variation by the expense of higher convergence period. The reference stress σ_{ref} is given by the expression

$$\sigma^i_{ref} = \left[\frac{\int_{V_T} \sigma^2_{eq} \, dV}{V_T} \right]^{1/2}_i \tag{6.2}$$

This formula describes how the elastic modulus at a location with the equivalent stress σ_{eq} (e.g. the von Mises equivalent stress) is updated from the i^{th} to the $(i+1)^{th}$ elastic iteration. This procedure continues until suitable convergence of a subsequent iteration is achieved.

In EMAP, during the second and subsequent linear elastic FEA, $\zeta_i = \frac{m^0}{m_L}$ changes with the change of elastic modulus of various elements. On the other hand, m^0 evaluated on the basis of total volume also decreases in subsequent linear elastic FEA except for the degenerate case, when m^0 would increase with the iteration violating the nesting surface theorem (Calladine and Drucker 1962).

6.3 The Proposed Iterative Method for Limit Load Estimation

The aim of EMAP is to redistribute the linear elastic stress distribution of i^{th} iteration by performing $(i+1)^{th}$ number of iteration. Therefore in subsequent linear elastic iterations it blunts all the peak stresses and eliminates all the kinematically inactive volume existing in the structure due to flaws, cracks, sharp notches, geometric discontinuities, concentrated load over a certain region etc. However blunting of peak stresses and a reference volume correction from the m_α-tangent construction plot ensures lower bound limit loads in all the linear elastic iterations.

6.3.1 Peak Stress Correction for $\zeta_i > 1+\sqrt{2}$

For a particular iteration, $\zeta_i > 1+\sqrt{2}$ indicates that peak stress exists in the stress distribution. The horizontal distance between $\zeta = 1+\sqrt{2}$ and $\zeta_{i=1} = \frac{m^0}{m_L}$ in Figure 3.5 signifies the amount of peak stress which has to be blunted. Therefore ζ_f of Eq. 3.19 can

be considered as, $\zeta_f = 1+\sqrt{2}$ after the peak stress correction. The m_α^T-multiplier expression of Eq. 3.20 becomes

$$m_\alpha{}^T = \frac{m^0}{\sqrt{2}} \tag{6.3}$$

6.3.2 Reference Volume Correction for $\zeta_i > 1+\sqrt{2}$

For a particular iteration $\zeta_i > 1+\sqrt{2}$ indicates that, kinematically inactive volume is existing in the stress distribution, which is not participating in the plastic action. Therefore, kinematically active volume based upper bound multiplier (m_{ref}^0) can be evaluated (derivation is given in Appendix D) for every iteration by projecting the linear elastic m^0 (which is m_2^0) at $\zeta = 1+\sqrt{2}$ as shown in Eq. 6.4, when $\zeta_i > 1+\sqrt{2}$. Therefore,

$$m_{ref}^0 = \frac{\sqrt{2}m_2^0}{\frac{1+\zeta_i^2}{2\zeta_i}} \tag{6.4}$$

Substituting the m^0 of Eq. 6.3 by the m_{ref}^0 of Eq. 6.4,

$$m_\alpha{}^T = \frac{m_2^0}{\frac{1+\zeta_i^2}{2\zeta_i}} \tag{6.5}$$

Therefore for iterations where $\zeta_i > 1+\sqrt{2}$, the m_α^T-multiplier is evaluated using Eq. 6.5

6.3.3 EMAP Flow Diagram for Limit Load Estimation

Reference volume and peak stress corrections has to be incorporated in order to obtain reasonable limit load multipliers. Figure 6.1 shows the proposed EMAP flow diagram for estimating the m_α^T-multipliers in subsequent linear elastic iterations. This algorithm systematically adjusts the elastic modulus of different elements in a finite element discretization scheme. This algorithm also utilizes the proposed m_α^T-multiplier expression when $\zeta_i > 1+\sqrt{2}$ in subsequent iterations in order to ensure lower bound m_α^T values in all the iterations. Once $\zeta_i \leq 1+\sqrt{2}$ value is reached, Eq. 3.17 is used for evaluating the m_α^T-multiplier in further iterations.

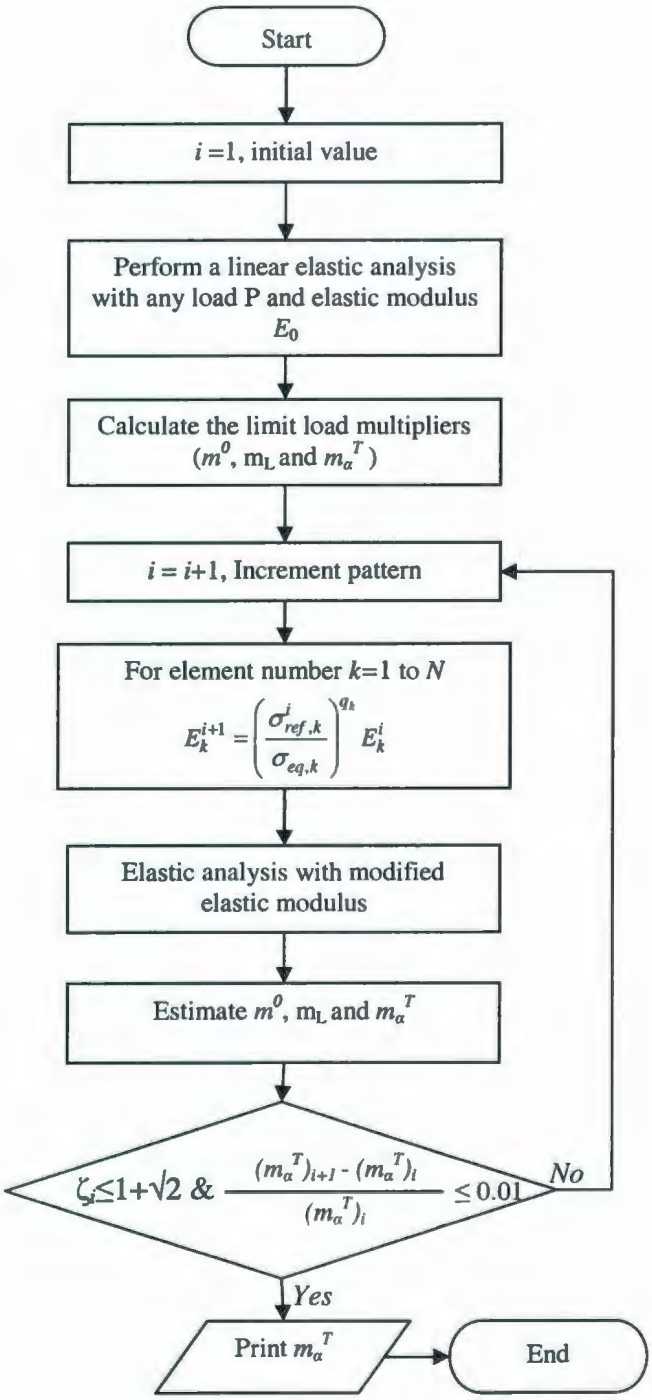

Figure 6.1 EMAP flow diagram for estimating limit load

In this algorithm, considerably smaller modulus adjustment parameter (q = 0.05) is used for EMAP in order to ensure good convergence which was reported by Adibi-Asl *et al.* (2006). For several geometric configurations, loading, and boundary conditions evaluation of m_α^T-multiplier based on EMAP has worked out well, as explained in the numerical example section. In order to simulate the plastic incompressibility condition, Poisson's ratio is chosen to be 0.47.

6.3.4 Convergence of the Multiplier $m_\alpha{}^T$ in Proposed Algorithm

The exact limit load multiplier (m) for most practical components and structures being analyzed is not known a priori. In the proposed algorithm a reference volume correction for regions of peak stresses is incorporated to ensure lower bound m_α-tangent values in all the linear elastic iterations. The convergence of limit load multiplier ($m_\alpha{}^T$-multiplier) in the proposed algorithm is shown in Figure 6.2 along with the basic upper bound and lower bound multipliers. With respect to Figure 6.2, the following can be stated:

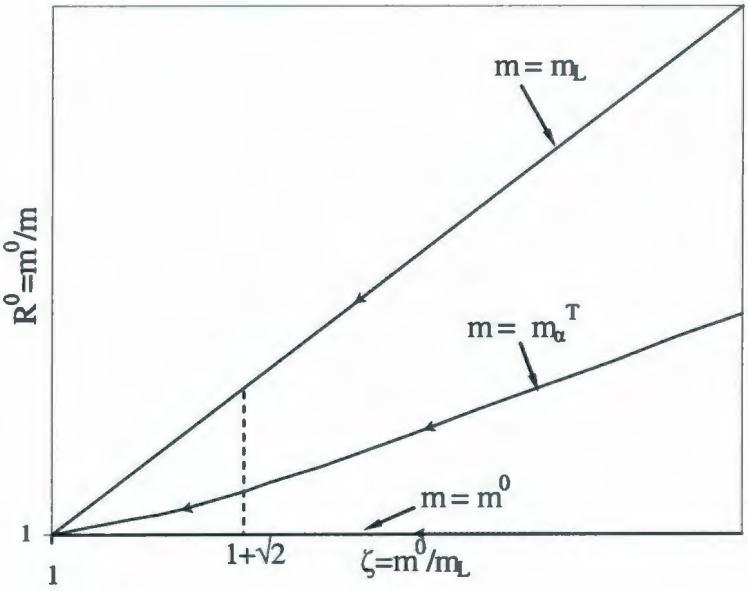

Figure 6.2 Convergence of limit load multipliers

1. When $m \to m_L$, the domain of statically admissible m^0 is bounded by the 45-deg (R^0 (max)) line and the positive x-axis.

2. When $m \to m^0$, the domain of the statically admissible m^0 is represented by the line $m = m^0$.

Therefore m_L and m^0 converges towards the limit state along the line $m = m_L$ and $m = m^0$ respectively. Similarly, m_α^T converges towards the limit state along the $m = m_\alpha^T$ trajectory in the context of iterative EMAP as shown in Figure 6.2. In this method it is assumed that the reduction of m^0 along the $m = m_\alpha^T$ trajectory implicitly accounts for the reference volume.

6.4 Numerical Examples

In this section, limit load estimates are determined for a number of ship structural components. All these ship structure components are described in chapter 5. For each component the m_α^T-multiplier is computed based on iterative linear elastic algorithm shown in Figure 6.1. Inelastic finite element analysis is performed as well in order to validate the results based on the procedure described in chapter 5.

6.4.1 Fixed End Beam

An initial linear elastic finite element analysis is performed and from the stress distribution of initial elastic FEA, m^0 and m_L are evaluated. Since $\zeta_{i=1} = 4.498$ is greater than $1+\sqrt{2}$, therefore significant amount of inactive volume or peak stresses or a combination of both is present in the stress distribution. Systematic elastic modulus adjustment (as directed in Figure 6.1) in subsequent iterations ensures proper reference volume correction and peak stress redistribution and thus generates an inelastic-like stress distribution. The variation of limit load multipliers with iterations is shown in Figure 6.3. It is evident from the figure that, all the limit load multipliers converge towards exact multiplier with iterations and the convergence of the m_α^T-multiplier is much faster in compared to other limit load multipliers. The m_α^T-multiplier at the end of the iteration is evaluated as $m_\alpha^T = 2.130$. Then a nonlinear finite element analysis is performed, which gives the limit load multiplier m_{NFEA}=2.154. The analytical solution (Burgreen, 1975) of the problem gives the limit load multiplier $m_{Analyt.} = 2.069$.

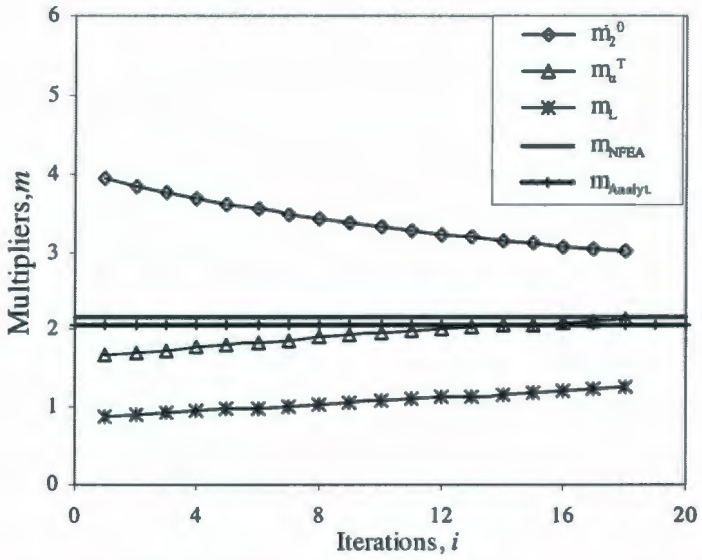

Figure 6.3 Variation of limit load multipliers for fixed end beam

6.4.2 Transverse Ship Frame Subjected to Hydrostatic Pressure

An initial linear elastic finite element analysis is performed and from the stress distribution of initial elastic FEA, m^0 and m_L are evaluated. Since $\zeta_{i=1}$ =8.799 is greater than $1+\sqrt{2}$, therefore either significant amount of inactive volume or pseudo peak stresses or a combination of both is present in the stress distribution. Systematic elastic modulus adjustment (as directed in Figure 6.1) in subsequent iterations ensures proper reference volume correction and peak stress redistribution and thus generates an inelastic-like stress distribution. Variation of limit load multipliers with iterations is shown in Figure 6.4. It is evident from the figure that, all the limit load multipliers converge towards exact multiplier with number of iterations and the convergence of the $m_\alpha{}^T$-multiplier is much faster in compared to other limit load multipliers. The $m_\alpha{}^T$-multiplier

at the end of the iteration is evaluated as m_α^T=1.147. Then a nonlinear finite element analysis is performed, which gives the limit load multiplier m_{NFEA} = 1.155.

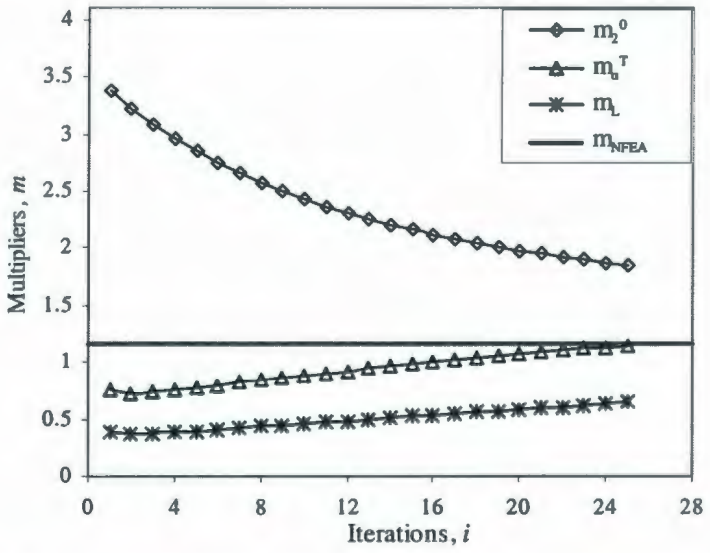

Figure 6.4 Variation of limit load multipliers for transverse ship frame

6.4.3 Rectangular plate under uniform pressure

Plates are one of the most important components of ship structures. A simply supported rectangular plate with length 2000 mm; width 800 mm and thickness 10 mm is modeled (detailed description is given in section 5.2.3). The variation of limit load multipliers with iterations is shown in Figure 6.5. It is evident from the figure that the upper bound and lower bound limit load multipliers converge towards exact multiplier with number of iterations. Moreover m_α^T-multiplier is almost invariant with number of iterations for this problem which signifies that there is negligible amount dead volume and peak stress present in the structure and the m_α^T-multiplier is evaluated as m_α^T=0.921.

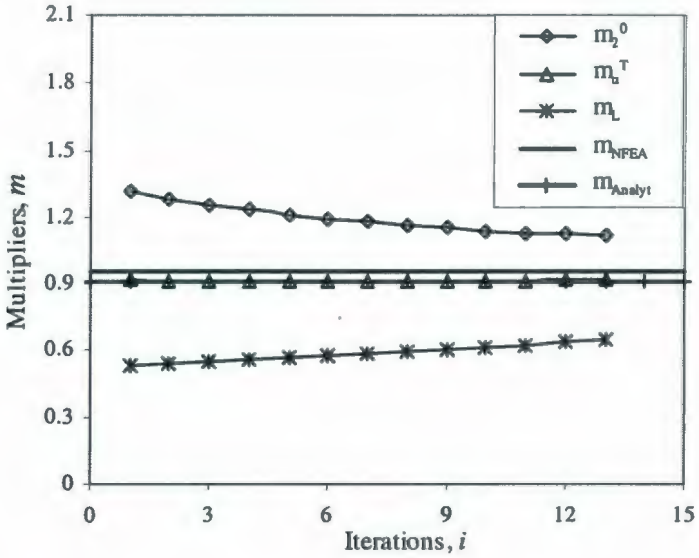

Figure 6.5 Variation of limit load multipliers for simply supported plate

Then a nonlinear finite element analysis is performed, which gives the limit load multiplier m_{NFEA}=0.952. The analytical solution (Sobotka, 1989) of the problem gives the limit load multiplier $m_{Analyt.} = 0.909$.

6.4.4 Single Stiffened Plate of Ship Structure

An initial linear elastic finite element analysis is performed and from the stress distribution of initial elastic FEA, m^0 and m_L are evaluated. Since $\zeta_{i=1} = 3.073$ is greater than $1+\sqrt{2}$, therefore either significant amount of inactive volume or pseudo peak stresses or a combination of both is present in the stress distribution. Systematic elastic modulus adjustment (as directed in Figure 6.1) in subsequent iterations ensures proper reference volume correction and peak stress redistribution and thus generates an inelastic-like stress distribution. Variation of limit load multipliers with iterations is shown in

Figure 6.6. It is evident from the figure that, all the limit load multipliers converge towards exact multiplier with number of iterations and the convergence of the m_α^T-multiplier is much faster in compared to other limit load multipliers. The m_α^T-multiplier at the end of the iteration is evaluated as m_α^T=2.630. Then a nonlinear finite element analysis is performed, which gives the limit load multiplier m_{NFEA} = 2.663.

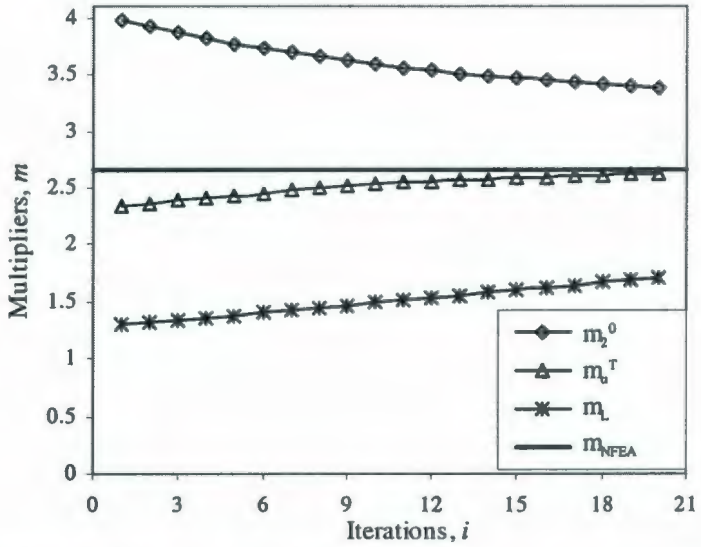

Figure 6.6 Variation of limit load multipliers for single stiffened plate

6.4.5 Small Grillage of Ship Structure

An initial linear elastic finite element analysis is performed. From the stress distribution of initial elastic FEA, m^0 and m_L are evaluated. Since ζ_i =3.878 is greater than $1+\sqrt{2}$, therefore either significant amount of inactive volume or pseudo peak stresses or a combination of both is present in the stress distribution. Systematic elastic modulus adjustment (as directed in Figure 6.1) in subsequent iterations ensures proper reference volume correction and peak stress redistribution and thus generates an inelastic-like stress

distribution. Variation of limit load multipliers with iterations is shown in Figure 6.7. It is evident from the figure that, all the limit load multipliers converge towards exact multiplier with number of iterations and the convergence of the m_α^T-multiplier is much faster in compared to other limit load multipliers. The m_α^T-multiplier at the end of the iteration is evaluated as $m_\alpha^T = 5.896$. Then a nonlinear finite element analysis is performed, which gives the limit load multiplier $m_{NFEA} = 5.915$.

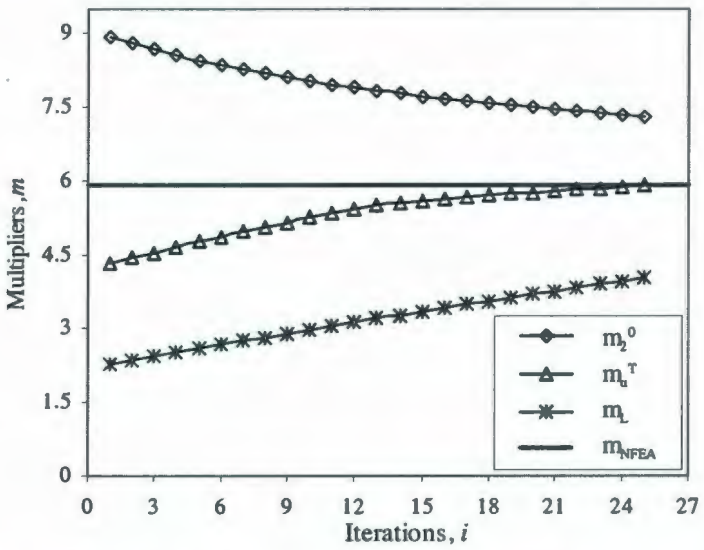

Figure 6.7 Variation of limit load multipliers for small grillage of ship structure

6.4.6 Large Grillage of Ship Structure

An initial linear elastic finite element analysis is performed. From the stress distribution of initial elastic FEA, m^0 and m_L are evaluated. Since $\zeta_i = 6.050$ is greater than $1+\sqrt{2}$, therefore either significant amount of inactive volume or pseudo peak stresses or a combination of both is present in the stress distribution. Systematic elastic modulus adjustment (as directed in Figure 6.1) in subsequent iterations ensures proper reference

volume correction and peak stress redistribution and thus generates an inelastic-like stress distribution. Variation of limit load multipliers with iterations is shown in Figure 6.8. It is evident from the figure that, all the limit load multipliers converge towards exact multiplier with number of iterations and the convergence of the m_α^T-multiplier is much faster in compared to other limit load multipliers. The m_α^T-multiplier at the end of the iteration is evaluated as m_α^T=3.763. Then a nonlinear finite element analysis is performed, which gives the limit load multiplier m_{NFEA} = 3.769.

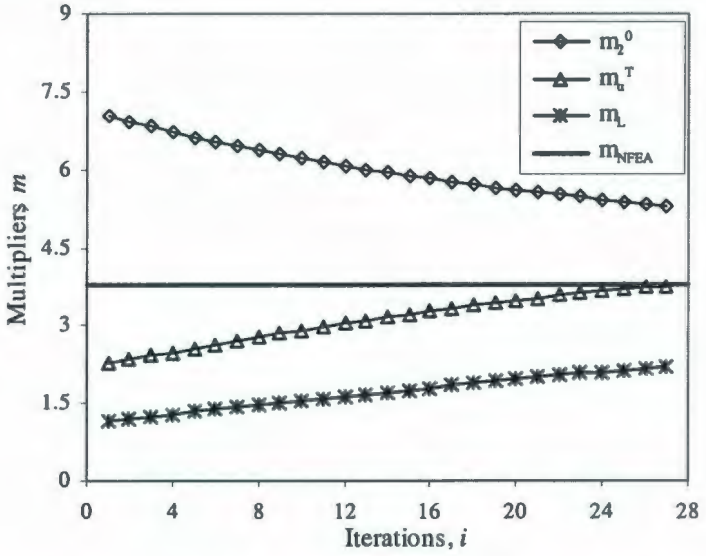

Figure 6.8 Variation of limit load multipliers for large grillage of ship structure

6.5 Discussion

Evaluation of the m_α^T-multiplier based on initial linear elastic analysis (Seshadri and Hossain 2009) using Eq. 3.20 is a function of m^0 obtained from the initial linear elastic analysis and ζ_f. The m^0 calculation may have dead volume effect and thus may result in

m_α^T-multiplier being an upper bound. On the other hand, presence of any peak stress may result in m_α^T-multiplier to be conservative. However, in EMAP based m_α^T-multiplier evaluation algorithm (Figure 6.1), ζ reaches a value less than or equal to $1+\sqrt{2}$, which implicitly accounts for the dead volume and peak stress correction and thus ensures that m_α^T-multiplier is very close to the exact limit load multiplier . Results of different analyses for the aforementioned problems are summarized in Table 6.1.

Table 6.1 Comparison of limit load multipliers for different components

Problem	Initial linear elastic FEA of EMAP (m_α^T multiplier)	Final linear elastic FEA of EMAP (m_α^T multiplier)	Inelastic FEA m_{NFEA}	Analytical $m_{Analyt.}$
Fixed Beam (Figure 5.1)	1.668	2.130	2.154	2.069
Trans. Frame (Figure 5.2)	0.758	1.147	1.155	-
Simp. Supp. Plate (t=10 mm)	0.917	0.921	0.952	0.909
Stiffened Plate (Figure 5.4)	2.343	2.630	2.663	-
Small Grillage (Figure 5.5)	4.312	5.896	5.915	-
Large Grillage (Figure 5.6)	2.268	3.763	3.769	-

6.6 Conclusion

In this chapter, a simplified algorithm of limit analysis is proposed by combining the m_α-tangent method with the elastic modulus adjustment procedure. Then the algorithm is

implemented for the limit load analysis of different ship structure components. Inelastic-like stress and strain distribution has been generated by the redistribution of elastic stresses on the basis of EMAP in an iterative scheme and $m_\alpha{}^T$-multiplier is evaluated from that stress field.

The EMAP based $m_\alpha{}^T$-multiplier is found to be very close to the exact limit load multipliers for all the above mentioned ship structure components. The integration of the m_α-Tangent method with EMAP also ensures faster convergence toward the exact limit load multiplier even for a very small convergence parameter (q). Therefore EMAP based $m_\alpha{}^T$-multiplier can be used as an alternative to the inelastic multiplier in the limit analysis of ship structure components.

CHAPTER 7

SINGLE ELASTIC ANALYSIS BASED LIMIT ANALYSIS

7.1 Introduction

Proper identification of kinematically active volume is an important step in the evaluation of an accurate limit load multiplier. The m_α^T-multiplier is a function of upper bound and lower bound multiplier. Therefore the upper bound and the lower bound multiplier has to be estimated properly in order to ensure the accuracy of the m_α^T-multiplier. The upper bound multiplier is affected by the kinematically inactive volume of the single linear elastic stress field; on the other hand the lower bound multiplier is affected by the peak stress of that linear elastic stress field. Seshadri and Hossain (2009) have proposed the peak stress blunting procedure which is discussed in chapter 3. This chapter focuses on

the characteristics of the m_α-tangent construction plot due to the inclusion of the reference volume as an additional feature, as discussed in chapter 4. This chapter also includes the evaluation of lower bound limit load for ship structure components based on a single linear elastic analysis by using the m_α-tangent method with its reference volume feature. Inelastic finite element and some analytical limit analysis results are also included for the purpose of comparison.

7.2 The m_α^T Multiplier for Different Class of Components

Seshadri and Adibi-Asl (2007) has shown that, two-bar model (TBM), is the simplest structure in which stress redistribution occurs after the onset of yielding. As such, it serves as a simplified representation of similar redistribution phenomena in any mechanical or ship structure component. The geometry of the TBM can be adapted to best reflect the behavior of the component. Utilizing this concept in conjunction with the m_α-tangent construction, Seshadri and Hossain (2009) categorized the components into two classes in terms of peak stress existence as discussed earlier (section 3.4). However, the inclusion of reference volume feature with the m_α-tangent method categorizes the components into following two classes based on single linear elastic analysis.

7.2.1 Presence of Negligible Peak Stresses and Inactive Volume, $\zeta_{i=1} \leq 1+\sqrt{2}$

The $m_\alpha{}^T$ multiplier for the components having ζ_i in the range of $1 \leq \zeta_{i=1} \leq 1+\sqrt{2}$, can be evaluated using Eq. (3.17) as discussed earlier. For these components m^0 and m_L obtained from the single linear elastic can be directly used in the $m_\alpha{}^T$ multiplier expression (Eq. (3.17)). Components having negligible amount of peak stresses and inactive volume into their initial elastic stress distribution are in this category.

7.2.2 Presence of Significant Peak Stresses and Inactive Volume, $\zeta_{i=1} > 1+\sqrt{2}$

For components having $\zeta_{i=1} > 1+\sqrt{2}$ it is necessary to make both the peak stress and dead volume corrections prior to evaluating the $m_\alpha{}^T$ multiplier. Peak stress correction is related to ζ_i correction and dead volume correction is related to the correction of m^0. Seshadri and Hossain (2009) extended the $m_\alpha{}^T$-multiplier for the components having significant amount peak stress (Eq.3.20).

The kinematically active reference volume based upper bound multiplier (m^0_{ref}) is explained in section 4.5 (Eq. 4.9). Using m^0_{ref} (from Eq. 4.9) and ζ_f (from Eq. 3.19), $m_\alpha{}^T$-multiplier expression can be evaluated as

$$m_\alpha{}^T = \frac{m^0_{ref}}{1+\left(1-\frac{1}{\sqrt{2}}\right)(\zeta_f - 1)} \tag{7.1}$$

For some geometric transitions for which $\zeta_i > 1+\sqrt{2}$, redistribution of secondary stresses could occur along with peak stresses. In such cases, the value of m^0 may be not constant during the blunting of peak stresses, and there is a gradual reduction in its magnitude. These cases are usually attributed to components undergoing highly localized plastic flow such as beam and frame structures.

7.3 Graphical Representation of the m_α^T Multiplier

For the purpose of graphical representation, it is convenient to rewrite the solution for m_α^T in terms of the normalized multipliers that were introduced earlier, i.e. with $R_\alpha^T = \frac{m_\alpha^T}{m}$, Eq. 3.17 becomes

$$R_\alpha^T = \frac{R^0}{1+\left(1-\frac{1}{\sqrt{2}}\right)\left(\frac{R^0}{R_L}-1\right)} \tag{7.2}$$

The multiplier m is exact limit load multiplier which is not known in priori and its estimation is the final goal. By using the exact multiplier m, the above normalized variables can be defined:

$$R_L = \frac{m_L}{m}, \quad R^0 = \frac{m^0}{m}, \; \zeta = \frac{m^0}{m_L} = \frac{R^0}{R_L}$$

Now considering $m = m_\alpha^T$ (i.e. $R_\alpha^T = 1$), Eq. 7.2 becomes

$$R^0 = 1+\left(1-\frac{1}{\sqrt{2}}\right)(\zeta - 1) \tag{7.3}$$

Eq. 7.3 can be graphically represented in a two dimensional space (R^0 vs ζ space) which is shown in Figure 7.1 by $R_\alpha^T = 1$ line. Similarly the $m = m_\alpha^T$ trajectory shown in Figure 7.1 is the graphical representation of Eq. 7.4 which is obtained by normalizing Eq. 3.20 with the exact multiplier m. This trajectory location is governed by the peak stress correction as discussed earlier and therefore can be utilized for the components having significant amount peak stress.

$$R^0 = 1 + \left(1 - \frac{1}{\sqrt{2}}\right)\left((1 + 0.2929\,(\zeta - 1)) \pm \sqrt{(1 + 0.2929\,(\zeta - 1))^2 - 1} - 1\right)) \qquad (7.4)$$

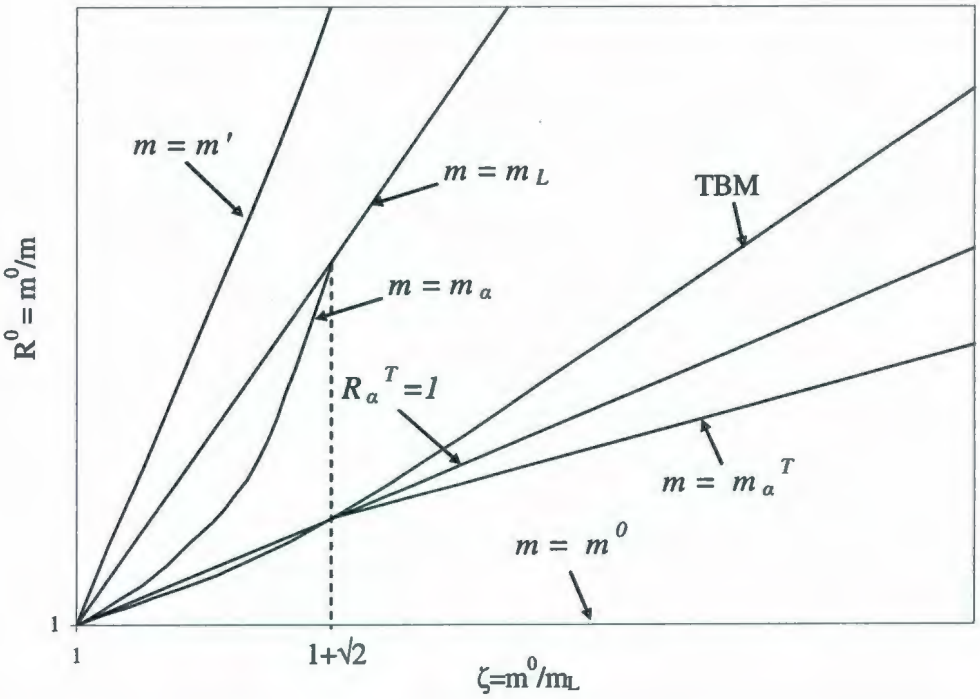

Figure 7.1 The m_α^T multiplier representation with peak stress correction only

In order to incorporate the kinematically inactive volume correction along with the peak stress correction, Eq. 7.1 has to be plotted in the two dimensional space of R^0 vs ζ. Rearranging Eq. 7.1 expression such that ζ becomes a function of R^0:

$$R^0 = \frac{\left[1+\zeta^2\right]\left[1+\left(1-\frac{1}{\sqrt{2}}\right)\left((1+0.2929\,(\zeta-1))\pm\sqrt{(1+0.2929\,(\zeta-1))^2-1}-1\right)\right]}{\zeta\left(\sqrt{2}\zeta\left(\sqrt{2}-1\right)+\sqrt{2}\right)} \qquad (7.5)$$

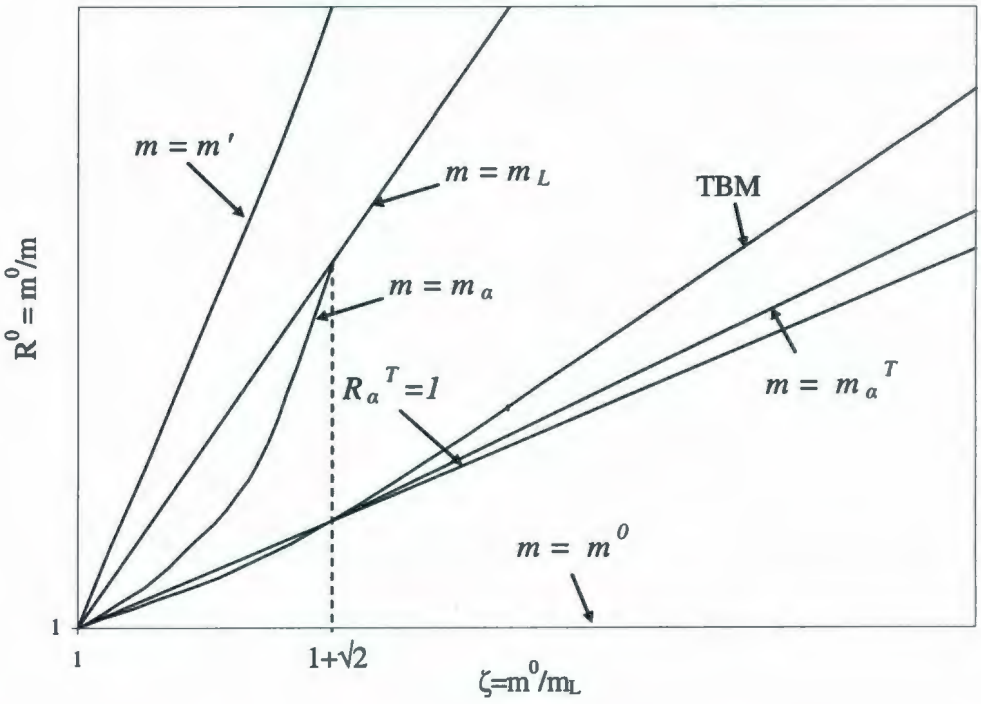

Figure 7.2 The $m_\alpha^{\ T}$ multiplier representation with reference volume correction

Comparing Figure 7.1 with Figure 7.2 it is evident that peak stress correction locates the $m = m_\alpha^T$ trajectory below the $R_\alpha^T = 1$ line, on the other hand, kinematically inactive volume correction along with the peak stress correction locates the $m = m_\alpha^T$ trajectory

above the $R_\alpha^T = 1$ line. The divergence between them is therefore the amount of uncorrected percentage of upper bound multiplier for a particular ζ location. Therefore the $m = m_\alpha^T$ trajectory of Figure 7.1 ensures lower boundedness of the $m_\alpha{}^T$ multiplier for the components having only significant amount peak stress presence into them; on the other hand, the $m = m_\alpha^T$ trajectory of Figure 7.2 ensures lower boundedness of the $m_\alpha{}^T$ multiplier for the components having peak stress as well as inactive volume existence into them.

7.4. NUMERICAL EXAMPLES

In this section, limit load estimates are determined for a number of ship structural components. All the problems are modeled using the ANSYS 11.0 software. For each component the $m_\alpha{}^T$-multiplier is computed based on a single linear elastic analysis. Inelastic finite element analysis is performed as well using an elastic-perfectly-plastic material model.

7.4.1 Fixed End Beam

At first initial linear elastic finite element analysis is performed for the fixed end beam discussed in section 5.2.1. From the results of initial elastic FEA, m^0 and m_L are evaluated. Since $\zeta_i = 4.498$ is greater than $1+\sqrt{2}$, therefore significant amount of inactive volume and peak stresses are considered to be present in the structure. Now m_{ref}^0 is evaluated (Eq. 4.9) so that ζ *at* B' and B (Figure 3.5) are equal. Similarly ζ_f is

evaluated (Eq. 3.19) so that m^0 *at* B and B'' (Figure 3.5) are equal. Eq. 7.1 is used to calculate the value of m_α^T using $m_{ref}^0 = 3.378$, $\zeta_f = 3.785$ and found to be 1.860. Then an inelastic finite element analysis is performed, which gives the limit load multiplier m_{NFEA}=2.154. The analytical solution (Burgreen, 1975) of the problem gives the limit load multiplier $m_{Analytical} = 2.069$. Results are summarized in Table 7.1.

Table 7.1 Limit load multipliers for fixed end beam

m^0	m_L	m^0/m_L	$m^0{}_{ref}$	ζ_f	m_α^T	m^{NFEA}	$m_{Analytical}$
3.937	0.875	4.498	3.378	3.785	1.860	2.154	2.069

7.4.2 Transverse Ship Frame Subjected to Hydrostatic Pressure

At first initial linear elastic finite element analysis is performed for the transverse ship frame discussed in section 5.2.2. Values for m^0 and m_L are obtained using an initial elastic FEA. Since $\zeta_i = 8.799$ is greater than $1+\sqrt{2}$, therefore significant amount of inactive volume and peak stresses are considered to be present in the structure based on Figure 3.5. Now m_{ref}^0 is evaluated (Eq. 4.9) so that ζ *at* B' and B (Figure 3.5) are equal. Similarly ζ_f is evaluated (Eq. 3.19) so that m^0 *at* B and B'' (Figure 3.5) are equal. Eq. 7.1 is used to calculate the value of m_α^T using $m_{ref}^0 = 2.490$, $\zeta_f = 6.413$ and found to be 0.963. Then an inelastic finite element analysis is performed, which gives the limit load multiplier m_{NFEA}=1.155. Results are summarized in Table 7.2.

Table 7.2 Limit load multipliers for transverse ship frame

m^0	m_L	m^0/m_L	$m^0{}_{ref}$	ζ_f	$m_a{}^T$	m^{NFEA}
3.378	0.384	8.799	2.490	6.413	0.963	1.155

7.4.3 Rectangular plates under uniform pressure

Plates are one of the most important components of ship structures. Plates of three different dimensions and two different boundary conditions (as discussed in section 5.2.3) are analyzed based on initial linear elastic finite element analysis. Inelastic finite element analyses are also performed and analytical solutions (Sobotka, 1989) have been evaluated. Results are summarized in Table 7.3.

Table 7.3 Limit load multipliers for rectangular plates

(a) All edges simply supported

Thickness (mm)	m^0	m_L	m^0/m_L	$m^0{}_{ref}$	ζ_f	$m_a{}^T$	m_{NFEA}	$m_{Analytical}$
10	1.312	0.534	2.456	1.307	2.444	0.919	0.952	0.909
15	2.871	1.167	2.460	2.860	2.447	2.009	2.133	2.045
20	5.090	2.011	2.531	5.039	2.496	3.504	3.794	3.635

(b) All edges fixed

Thickness (mm)	m^0	m_L	m^0/m_L	$m^0{}_{ref}$	ζ_f	$m_a{}^T$	m_{NFEA}	$m_{Analytical}$
10	2.976	0.815	3.653	2.694	3.246	1.625	2.030	1.817
15	6.662	1.778	3.747	5.990	3.307	3.575	4.359	4.089
20	11.781	3.064	3.844	10.523	3.370	6.212	7.178	7.269

7.4.4 Single Stiffened Plate of Ship Structure

At first initial linear elastic finite element analysis is performed for the transverse ship frame discussed in section 5.2.4. From the results of initial elastic FEA, m^0 and m_L are evaluated. Since $\zeta_i = 3.073$ is greater than $1+\sqrt{2}$, therefore significant amount of inactive volume and peak stresses are considered to be present in the structure based on Figure 3.5. Now m^0_{ref} is evaluated (Eq. 4.9) so that ζ *at* B' and B (Figure 3.5) are equal. Similarly ζ_f is evaluated (Eq. 3.19) so that m^0 at B and B'' (Figure 3.5) are equal. Eq. 7.1 is used to calculate the value of m_α^T using $m^0_{ref} = 3.765$, $\zeta_f = 2.865$ and found to be 2.435. Then an inelastic finite element analysis is performed, which gives the limit load multiplier m_{NFEA}=2.663. Results are summarized in Table 7.4.

Table 7.4 Limit load multipliers for single stiffened plate

m^0	m_L	m^0/m_L	$m^0{}_{ref}$	ζ_f	m_α^T	m^{NFEA}
3.981	1.295	3.073	3.765	2.865	2.435	2.663

7.4.5 Small Grillage of Ship Structure

At first initial linear elastic finite element analysis is performed for the small grillage discussed in section 5.2.5. From the results of initial elastic FEA, m^0 and m_L are evaluated. Since $\zeta_i = 3.878$ is greater than $1+\sqrt{2}$, therefore significant amount of inactive volume and peak stresses are considered to be present in the structure based on Figure 3.5. Now m^0_{ref} is evaluated (Eq. 4.9) so that ζ *at* B' and B (Figure 3.5) are equal. Similarly ζ_f is evaluated (Eq. 3.19) so that m^0 *at* B and B'' (Figure 3.5) are equal. Eq. 7.1

is used to calculate the value of m_α^T using $m_{ref}^0 = 7.946$, $\zeta_f = 3.391$ and found to be 4.673. Then an inelastic finite element analysis is performed, which gives the limit load multiplier m_{NFEA} =5.915. Results are summarized in Table 7.5.

Table 7.5 Limit load multipliers for small grillage

m^0	m_L	m^0/m_L	$m^0{}_{ref}$	ζ_f	m_α^T	m^{NFEA}
8.916	2.299	3.878	7.946	3.391	4.673	5.915

7.4.6 Large Grillage of Ship Structure

An initial linear elastic finite element analysis is performed. From the results of initial elastic FEA, m^0 and m_L are evaluated. Since ζ_i =6.050 is greater than $1+\sqrt{2}$, therefore significant amount of inactive volume and peak stresses are considered to be present in the structure based on Figure 3.5. Now m_{ref}^0 is evaluated (Eq. 4.9) so that ζ *at B'* and *B* (Figure 3.5) are equal. Similarly ζ_f is evaluated (Eq. 3.19) so that m^0 *at B* and *B"* (Figure 3.5) are equal. Eq. 7.1 is used to calculate the value of m_α^T using $m_{ref}^0 = 5.623$, $\zeta_f = 4.748$ and found to be 2.680. Then an inelastic finite element analysis is performed, which gives the limit load multiplier m_{NFEA} =3.769. Results are summarized in Table 7.6.

Table 7.6 Limit load multipliers for large grillage

m^0	m_L	m^0/m_L	$m^0{}_{ref}$	ζ_f	m_α^T	m^{NFEA}
7.048	1.165	6.050	5.623	4.748	2.680	3.769

7. 5 Discussion and Conclusions

The m_α-tangent method presented in this chapter provides approximate estimates for the limit loads of ship structure components based on a single linear elastic analysis. The method makes use of the "limiting tangent" in order to relate the initial elastic state of a component or structure to that of the exact limit state. The estimates of the values of the upper bound multiplier m^0 and the classical lower bound multiplier m_L are obtained from the initial linear elastic analysis.

Figure 7.3 is the graphical representation of Eq. 7.5 where for a particular value of $\frac{m^0}{m_L}$, the m = $m_\alpha{}^T$ trajectory renders the result $(\frac{m^0}{m_\alpha{}^T})$ using the suggested method. The locations of the values of $\frac{m^0}{m_{NFEA}}$ for all the example problems presented are also shown on Figure 7.3. It is evident from the figure that at any value of $\frac{m^0}{m_L}$, the value of $\frac{m^0}{m_{NFEA}}$ for a component lies beneath the m = $m_\alpha{}^T$ trajectory, which indicates the lower bound nature of the m_α-tangent method after incorporating the reference volume correction.

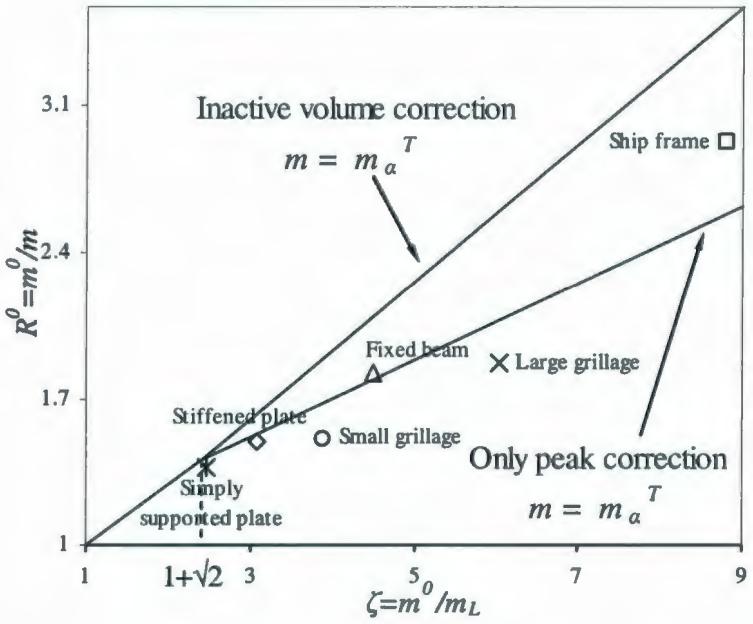

Figure 7.3 Location of nonlinear FEA results on the m_α-tangent plot

It should be noted that, the proposed methodology takes into consideration corrections as a result of the inactive volume and the peak stress, based on the m_α-tangent construction plot as shown in Figure 3.5. Therefore the $m_\alpha{}^T$-multiplier is either an exact or a lower bound multiplier. Thus, the methodology can be used as a basis for the safe design of ship structures components.

A comparison between the methods suggested in this work and the inelastic finite element approach is presented in Tables 7.7 and 7.8. Table 7.7 shows the advantages and limitations of different methods, while Table 7.8 gives a comparison between the computation times for different methods discussed in this thesis.

Table 7.7 Advantages and limitations of different limit analysis techniques

Analysis	Advantages	Limitations
Single linear elastic FEA based $m_\alpha{}^T$	1. Lower bound. 2. Rapid. 3. Simple to apply. 4. Applicable for many practical components and structures.	1. Accuracy of results is mesh dependent. 2. Large deflection features are needed to be incorporated with the method to extend its applicability.
EMAP based $m_\alpha{}^T$	1. Accurate. 2. Rapid. 3. Simple to apply. 4. Applicable for many practical components and structures.	1. Rate of convergence is dependant on q. 2. Accuracy of results is mesh dependent. 3. Large deflection features are needed to be incorporated with the method to extend its applicability.
Inelastic FEA m_{NFEA}	1. Accurate. 2. Applicable for many practical components and structures.	1. Time consuming. 2. Large data is needed to be analyzed. 3. Requires skilled personnel. 4. Numerical difficulties may be encountered. 5. Accuracy of results is mesh dependent.

Table 7.8 Approximate computation time required

Problem (time in minutes)	Single linear elastic FEA based $m_\alpha{}^T$	EMAP based $m_\alpha{}^T$	Inelastic FEA m_{NFEA}
Fixed Beam (Figure 5.1)	1	18	126
Trans. Frame (Figure 5.2)	2	25	180
Simp. Supp. Plate (t=10 mm)	6	78	2160
Stiffened Plate (Figure 5.4)	10	200	3600
Small Grillage (Figure 5.5)	10	250	3600
Large Grillage (Figure 5.6)	8	216	2880

It is quite clear from the above comparisons that although the inelastic finite element analysis renders accurate results but the method is fairly complicated and requires an exorbitant amount of computation time. The method suggested in this work provides conservative results which can be used to ensure safe design at a lower cost. The method suggested is simple, reliable and cost efficient.

CHAPTER 8

CONCLUSIONS AND FUTURE RESEARCH

8.1 Summary and Conclusions

Evaluation of maximum load carrying capacity of ship structure components and their integrity assessments are of paramount importance in ship building industries. Limit analysis is particularly important as it provides a guaranteed margin of safety against the failure of the structures. Development of simplified limit analysis techniques are of considerable interest due to their robustness and cost effectiveness over the conventional limit analysis techniques. This thesis is dedicated to developing an algorithm to estimate sufficiently accurate load carrying capacity of ship structure components based on iterative linear elastic analysis and also to make lower bound estimate of limit load, based on a single linear elastic analysis. Significant effort has been directed in order to achieve

the goal. This section summarizes the effectiveness of the simplified methods and their advantages and limitations for the application to the ship structure components.

The EMAP based limit analysis algorithm developed in this thesis is shown to be useful in determining the limit loads of ship structure components. This method is found to be sufficiently accurate and the resulting variation is within 3% (in lower bound side) in comparison to inelastic finite element analysis (FEA). This algorithm ensures consistent variation of limit load multipliers with iterations even for complex three dimensional geometric models while performing iterative EMAP. This method is also found to be time efficient in comparison to inelastic FEA. It is simple to apply and applicable for many practical components and structures. This method also overcomes the potential numerical difficulties encountered in inelastic FEA. Therefore, it can be considered as an attractive alternative over conventional inelastic finite element method. This method can also be considered as an independent verification tool for conventional limit analysis techniques. However the limitations of the method are, the accuracy of results is mesh dependent and rate of convergence is dependant on the convergence parameter q, although the convergence rate is boosted by the faster convergence tendency of the $m_\alpha{}^T$-multiplier.

The suggested m_α-Tangent method based on single linear elastic analysis can return lower bound results very rapidly in comparison to inelastic FEA as well EMAP based limit analysis. This method is also simple to apply, free from numerical difficulties and applicable for many practical components and structures. Therefore this method is

attractive for designing and sizing the ship structure components. However the limitations of the method are, it renders slightly lower bound result (resulting variation is within 20% in comparison to inelastic FEA) and the accuracy of results is mesh dependent.

The above mentioned methods are implemented to several ship structure components. It is quite clear that, although the inelastic finite element analysis gives accurate results, it is fairly complicated, mesh dependent, needs highly skilled personnel for proper implementation, requires an exorbitant amount of computational time and involves numerical difficulties which are discussed earlier.

8.2 Original Contributions

This section summarizes the original contributions of this thesis.

1. The m_α-Tangent method is combined with EMAP and an algorithm has been developed in order to estimate the maximum load carrying capacity of ship structure components based on iterative linear elastic analysis.

2. The m_α-Tangent method is also applied to a number of complex ship structure components based on single linear elastic analysis.

3. Reference volume correction has been incorporated to the m_α-Tangent method as an additional feature and it is implemented to single linear elastic analysis as well as iterative linear elastic analysis while performing simplified limit analysis.

4. A variety of ship structure components have been modeled and each model has been analyzed on the basis of the developed simplified techniques as well as the inelastic finite element analysis in order to estimate their maximum load carrying capacity.

5. The m_α-Tangent method based on a single linear elastic analysis is found to be even more rapid and simple in comparison to the proposed iterative EMAP based limit analysis algorithm and it also ensures lower bound load carrying capacity, which is always safe for design purpose.

6. The faster convergence tendency of the m_α^T-multiplier towards the exact limit load multiplier with iteration is also reported in comparison to other existing limit load multipliers.

8.3 Recommendations for Future Research

Recommendations for future work are as follows:

1. Simplified limit analysis techniques can be implemented to estimate the load carrying capacity of non homogeneous and anisotropic ship structure components.

2. The proposed techniques can be utilized in order to resolve the stress categorization in the ship structure components.

3. These methods can be implemented for the fitness for service assessment of ship structure components possessing corrosion damage.

4. The proposed methods can be implemented in order to perform the integrity assessment of in-service ship structure components.

5. These methods can be extended to the analysis of instability under compressive loads by taking care of the large deflection features into the problem formulation.

6. Application of the methods to some other complicated three dimensional models for example ship hulls, ship girders etc will also be beneficial.

REFERENCES

Adibi-Asl, R., Fanous, I. F. Z., Seshadri, R., 2006. Elastic Modulus Adjustment Procedures-Improved Convergence Schemes. Int. J. Pressure Vessels and Piping 83(2), 154-160.

Adibi-Asl, R., Seshadri, R., 2007. Simplified Limit Load Estimation of Components with Cracks Using the Reference Two-Bar Structure. ASME J. Pressure Vessel Technol. 131(1), 011204 (8 pages).

Ainsworth, R. A., Dean, D. W., and Budden, P. J. 2000. Development in Creep Fracture Assessments within the R5 Procedure, IUTAM Symposium on Creep in Structures, Nagoya, Japan, 321–330.

ANSYS, 2009 University Research Version 11.0, SAS IP, Inc.

ASME Boiler and Pressure Vessel Code, 2007, Section VIII, Division 2. New York: American Society of Mechanical Engineers.

British Standards, PD 6539. 1994. Guide to Methods for the Assessment of the Influence of Crack Growth on the Significance of Design in Component Operating at High Temperature, 1-37. London, UK: BSI.

Borrvall, T., 2009, A Heuristic Attempt to Reduce Transverse Shear Locking in Fully Integrated Hexahedra with Poor Aspect Ratio. 7th European LS-DYNA Conference. 14th - 15th of May 2009.

Burgreen, D., 1975. *Design Methods for Power Plant Structures.* C. P. Press Publishing

Caldwell, J.B. ,1965. Ultimate Longitudinal Strength. Transactions of RINA, Vol. 107, pp. 411-430

Calladine, C. R., 2000. *Plasticity for Engieers: Theory and Application. Chichester.* Horwood Publishing.

Calladine, C. R. and Drucker, D. C. 1962. Nesting Surfaces for Constant rate of Energy Dissipation in Creep. *Quarterly of Applied Mathematics, 20.* 79-84.

Claudia C., Marin-Artieda, Gary F. Dargush. 2007. Approximate Limit Load Evaluation of Structural Frames Using Linear Elastic Analysis. Journal of Engineering Structures. 29(2007), 296-304.

Cui, W., and Mansour, A.E. 1999. Generalization of a Simplified Method for Predicting Ultimate Compressive Strength of the Panels. International Shipbuilding Progress, Vol. 46(447), pp. 291-303.

Daley, C.G., Kendrick, A., and Appolonov, E. 2001. Plating and Framing Design in the Unified Requirements for Polar Class Ships. Proceedings of the 16th International Conference on Port and Ocean Engineering Under Arctic Conditions, Vol. 3, Ottowa, Canada, 779-91.

Drucker, D.C, 1957. Plastic Design Methods - Advantages ad Limitations, Trans SNAME, Vol. 65, pp. 172–96.

Drucker, D.C., Prager, W., and Greenberg, H.J., 1952. Extended Limit Design Theorems for Continuous Media. Quarterly Applied Mathematics, Vol. 9, pp. 381-389.

Fujikubo, M., Yao, T., Khedmati, M.R., Harada, M., and Yaagihara, D. 2005. Estimation of Ultimate Strength of Continuous Stiffeed Pael Under Combined Transverse Thurst and Lateral Pressure. Part 1: Continuous Plate. Marine Structures. Vol. 18(5-6), pp. 411-427.

Hong, L., and Amdahl, J. 2007. Plastic Design of Laterally Patch Loaded Plates for Ships. Marine Structures. Vol. 20, 124-142.

ISSC Report. 1997. Proceedings of 13th International Ship and Offshore Structures Congress. Vol. 1, 252-253. 18-22 August. Trondheim, Norway.

Jones, G. L., and Dhalla, A. K., 1981. Classification of Clamp Induced Stresses in Thin Walled Pipe. *Int. J. Pressure Vessels & Piping,* Vol. 81, pp. 17–23.

Mendelson, A. 1968. *Plasticity: Theory and Applications*. New York: MacMillan.

Mura, T., and Lee, S. L., 1963, "Application of Variational Principles to Limit Analysis," Quarterly of Applied Mathematics, Vol. 21, pp. 243–248.

Mura, T., Rimawi, W. H., and Lee, S. L. 1965. Extended Theorems of Limit Analysis. *Quarterly of Applied Mathematics, 23*, 171–179.

Naar, H., February 2000, *The Application of the Redistribution Node Method to Plastic Analysis of Ship Structures*, Thesis made in the ship laboratory of Helsinki university of technology.

Paik, J.K., and Mansour A.E., 1995. A Simple Formulation for Predicting the Ultimate Strength of Ships. Journal of Marine Science and Technology. Vol. 1, pp. 52-62.

Paik, J. K., and Pendersen, P. T., 1996. A Simplified Method for Predicting Ultimate Compressive Strength of Ship Panels. International Ship Building Progress, Vol. 43(434), pp. 139-157.

Paik, J.K., Thayamballi, A.K., and Kim, D.H., 1999. An Analytical Method for the Ultimate Compressive Strength and Effective Plating of Stiffened Panels. Journal of Constructional Steel Research, Vol. 49, pp. 43-68.

Paik, J.K., Thayamballi, A.K., and Kim, D.H., 2001. Advanced Ultimate Strength Formulations for Ship Plating Under Combined Biaxial Compression/Tension, Edge Shear, and Lateral Pressure Loads. Marine Technology, Vol. 38, No. 1, pp. 9-25.

Paik, J.K., Kim. B.J., and Seo, J.K., 2008a. Methods for Ultimate Limit State Assessment of Ships and Ship-Shaped Offshore Structures: Part I Un-stiffened Plates. Ocean Engineering, Vol. 35(2), pp. 261-270.

Paik, J.K., Kim. B.J., and Seo, J.K., 2008b. Methods for Ultimate Limit State Assessment of Ships and Ship-Shaped Offshore Structures: Part II Stiffened Panels. Ocean Engineering, Vol. 35(2), pp. 271-280.

Paik, J.K., Kim. B.J., and Seo, J.K., 2008c. Methods for Ultimate Limit State Assessment of Ships and Ship-Shaped Offshore Structures: Part III Hull Girders. Ocean Engineering, Vol. 35(2), pp. 281-286.

Pan, L., and Seshadri, R. 2002. Limit Load Estimation using Plastic Flow Parameter in Repeated Elastic Finite Element Analysis. J. Pressure Vessel Technology, 124, 433-439.

Reinhardt, W. D., and Seshadri, R. 2003. Limit Load Bounds for the m_α-Multiplier. J. Pressure Vessel Technology, 125, 11-18.

Sacchi G, and Save M., 1968, "On the Evaluation of the Limit Load for Rigid-Perfectly Plastic Continua," Meccanica, Vol. 3, pp. 199-206.

Schulte, C. A., 1960, Prediction of Creep Deflection of The Plastic Beam (*translated*). Proceedings ASTM, Vol. 60, pp. 895.

Seshadri, R., and Fernando, C. P. D, 1992. Limit Loads of Mechanical Components and Structures using the GLOSS R-Node Method. Transactions of the ASME: Journal of Pressure Vessel Technology, Vol. 114, pp. 201-208.

Seshadri, R., and Mangalaramanan, S.P. 1997. Lower Bound Limit Loads Using Variational Concepts: the m_α –Method. Int. J. Pressure Vessels & Piping, 71, 93-106.

Seshadri, R., and Hossain, M. M. 2009. Simplified Limit Load Determination using the m_α –Tangent Method. *J. Pressure Vessel Technol., 131*, 1-7.

"Ship Design and Construction", section 18.5, written by an International Group of Authorities, Thomas Lamb, Editor. Volume 1. Published in 2003, by The Society of Naval Architects and Marine Engineers, 601 Pavonia Ave, Jersey City, NJ, 07306.

Simonsen, B. C., *Mechanics of Ship Grounding*, Ph.D. thesis, Technical University of Denmark, Department of Naval Architecture and Offshore Engineering, February 1997.

Smith, C.S., 1976. Influence of Local Compressive Failure on Ultimate Longitudinal Strength of a Ship's Hull. Proceedings of International Symposium of Practical Design in Shipbuilding, Tokyo, Japan, 73-79.

Sobotka, Z., 1989. Theory of Plasticity and Limit Design of Plates. Elsevier, New York.

Webster, G., and Ainsworth, R. A. 1994. High Temperature Component Life Assessment. London: Chapman and Hall.

Xia, K., and Zhang Kenn K. Q., 2009. A Multiscale Finite Element Formulation for Axisymmetric Elastoplasticity with Volumetric Locking. Int. J. Numer. Anal. Meth. Geomech. Published online in Wiley Inter Science (www.interscience.wiley.com). DOI: 10.1002/nag.853.

Yao, T. 1996. Investigation into Longitudinal Strength of Ship Hull; Historical Review and State of the Art – Focusing on Ultimate Longitudinal Strength. Trans. West-Japan Soc. Naval Arch., No. 91, 221-252. (in Japanese).

Yao, T., and Nikolov, P.I., 1991. Progressive Collapse Analysis of a Ship's Hull Under Longitudinal Bending. Journal of the Society of Naval Architects of Japan, Vol. 170, 449-461.

Zyczkowski, M., 1981, *Combined loadings in the theory of plasticity,* Polish-Scientific Publication.

Appendix A

Derivation of m^0 Based on the Integral Mean of Yield

In limit analysis, the statically admissible stress field (equilibrium set) cannot lie outside the yield surface and the stress associated with a kinematically admissible strain rate field (compatibility set) in calculating the plastic dissipation should lie on the yield surface. Mura *et al.* (1965) proposed an approach that eliminates such a requirement and replaced it by the concept of '*integral mean of yield*' based on a variational formulation. The integral mean of yield criterion can be expressed as,

$$\int_{V_T} \mu^0 [f(\bar{s}_{ij}^0) + (\varphi^0)^2] dV = 0 \qquad \text{(A.1)}$$

Where $\bar{s}_{ij}^0$ corresponds to the stress state for impending plastic flow, φ^0 is a point function which assumes a value of zero at yield and remains positive below yield. The von Mises yield criterion is given by,

$$f(\bar{s}_{ij}) = \frac{3}{2}\bar{s}_{ij}^0 \bar{s}_{ij}^0 - \sigma_y^2 \qquad \text{(A.2)}$$

The flow parameter μ^0 is defined through the associated flow rule as,

$$\dot{\varepsilon}_{ij} = \mu\left(\frac{\partial f}{\partial s_{ij}}\right) \qquad \text{(A.3)}$$

Where $\mu \geq 0$ $(\mu^0 = \mu + \partial\mu)$ and $\dot{\varepsilon}_{ij}$ is the strain rate. Now $\bar{s}_{ij}^0 = m^0 s_{ij}^0$ where s_{ij}^0 represents the stress state for applied traction T_i.

Mura and co-workers have shown that m^0, μ^0 and φ^0 can be determined by rendering the functional F stationary in

$$F = m^0 - \int_{V_T} \mu^0 [f(\bar{s}_{ij}^0) + (\varphi^0)^2] dV \tag{A.4}$$

Leading to the set of equations

$$\frac{\partial F}{\partial m^0} = 0, \frac{\partial F}{\partial \mu^0} = 0, \frac{\partial F}{\partial \varphi^0} = 0 \tag{A.5}$$

For the von Mises yield criterion, Eq. (A.2), the functional becomes

$$F = m^0 - \int_{V_T} \mu^0 [\frac{3}{2}(m^0)^2 s_{ij}^0 s_{ij}^0 + (\varphi^0)^2] dV \tag{A.6}$$

Assuming a constant flow parameter μ^0 in Eq. (A.6) the solution of the functional becomes (Seshadri and Mangalaramanan, 1997),

$$m^0 = \frac{\sigma_y \sqrt{V_T}}{\sqrt{\int_{V_T} (\sigma_{eq})^2 dV}}, \ \varphi^0 = 0 \tag{A.7}$$

This expression takes all the plasticity effect into consideration.

Appendix B

Derivation of m_2^0 Expression

In classical limit analysis, the statically admissible stress field (equilibrium set) cannot lie outside the yield surface, and the stress associated with a kinematically admissible strain rate field in calculating the plastic dissipation should lie on the yield surface. Mura *et al.* (1965) proposed an approach to eliminate such a requirement, and replaced them with the concept of "integral mean of yield" in the context of a variational formulation. The integral mean of yield criterion can be expressed as

$$\int_{V_T} \mu^0 \left[f(\bar{s}_{ij}^0) + (\varphi^0)^2 \right] dV = 0 \tag{B.1}$$

The superscript "0" corresponds to a statically admissible state, and $\bar{s}_{ij}^0$ is a statically admissible deviatoric stress tensor close to an impending plastic collapse state. μ^0 is a flow parameter and φ^0 is a point function which can take on a value of zero at yield and remains positive below yield values.

We define $\bar{s}_{ij}^0 = s_{ij} + \delta s_{ij}$, where s_{ij} correspond to a state of impending collapse for which the von-Mises yield criterion is given by the expression

$$f(s_{ij}) = \frac{1}{2} s_{ij} s_{ij} - k^2 \tag{B.2}$$

Mura and co-workers have shown that m_2^0, μ^0 and φ^0 can be determined by rendering the functional F stationary in

$$F = m^0 - \int_{V_T} \mu^0 [f(s_{ij}) + (\varphi^0)^2] dV \tag{B.3}$$

Leading to the set of equations

$$\frac{\partial F}{\partial m^0} = 0, \frac{\partial F}{\partial \mu^0} = 0, \frac{\partial F}{\partial \varphi^0} = 0 \tag{B.4}$$

For an elastic-perfectly-plastic material, $k^2 = \sigma_y^2/3$ and $s_{ij}s_{ij}/2 = (\sigma_{eq})^2/3$ and at yield $\varphi^0 = 0$. Therefore the solution of the functional becomes (let $m^0 = m_2^0$),

$$\int_{V_T} \mu^0 \left[(m_2^0 \sigma_{eq})^2 - \sigma_y^2 \right] dV = 0 \tag{B.5}$$

Re-arranging Eq. (B.5) yields

$$m_2^0 = \sigma_y \sqrt{\frac{\int_{V_T} \mu^0 \, dV}{\int_{V_T} \mu^0 (\sigma_{eq})^2 \, dV}} \tag{B.6}$$

The associated flow rule can be expressed as

$$\dot{\varepsilon}_{ij} = \mu \left(\frac{\partial f}{\partial s_{ij}} \right) \tag{B.7}$$

Where $\mu \geq 0$ ($\mu^0 = \mu + \partial\mu$) and $\dot{\varepsilon}_{ij}$ is the strain rate. For elastic-perfectly-plastic Eq. (B.7) can be written as

$$\dot{\varepsilon}_{ij} = \mu^0 s_{ij} \tag{B.8}$$

Therefore, μ^0 can be defined as

$$\mu^0 = \frac{3\varepsilon_{eq}}{2\sigma_{eq}} \tag{B.9}$$

where $\sigma_{eq} = \sqrt{(3/2) s_{ij} s_{ij}}$ is equivalent stress and similarly $\varepsilon_{eq} = \sqrt{(2/3) \varepsilon_{ij} \varepsilon_{ij}}$ is equivalent strain. Therefore, the new upper bound multiplier m_2^0 is determined as

$$m_2^0 = \sigma_y \sqrt{\frac{\int_{V_T} \frac{\varepsilon_{eq}}{\sigma_{eq}} dV}{\int_{V_T} \sigma_{eq} \varepsilon_{eq} \, dV}} \Leftrightarrow \sigma_y \sqrt{\frac{\sum_{k=1}^{N} \left(\frac{\varepsilon_{eq}}{\sigma_{eq}} \Delta V \right)_k}{\sum_{k=1}^{N} \left(\sigma_{eq} \varepsilon_{eq} \, \Delta V \right)_k}} \qquad \text{(B.10)}$$

Appendix C

Derivation of Limiting Tangent

(a)Proof of $m = m_L$ line tangent to $m = m'$ curve at limit state

The expression of m' by normalizing with the best estimate multiplier m (usually unknown) can be represented as (see Eq. 3.7),

$$R' = \frac{2R^0}{1+\zeta^2} \tag{C.1}$$

In a two-dimensional space the $R' = 1$ line can be represented by plotting R^0 vs ζ based on Eq. (C.2) as shown in Figure 7.1.

$$R' = 1 = \frac{2R^0}{1+\zeta^2} \tag{C.2}$$

In order to obtain the slope of the tangent line for the curve at any ζ location, differentiate Eq. (C.2) with respect to ζ. The slope of the tangent line at limit state ($m^0 = m_L = m' = m$) can be obtained as,

$$\left(\frac{dR^0}{d\zeta}\right)_{\zeta=1} = 1 \tag{C.3}$$

This is the slope of the $m = m_L$ line as shown in Figure 7.1. Therefore $m = m_L$ is the tangent to $m = m'$ curve at limit state.

(b)Proof of $m = m^0$ line tangent to TBM trajectory at limit state

In a two-dimensional space the TBM trajectory can be represented (as shown in Figure 7.1) by plotting R^0 vs ζ based on the following equation:

$$R^0 = \frac{1+\zeta^2}{2\zeta} \tag{C.4}$$

In order to obtain the slope of the tangent line for the curve at any ζ location, differentiate Eq. (C.4) with respect to ζ. The slope of the tangent line at limit state can be obtained as,

$$\left(\frac{dR^0}{d\zeta}\right)_{\zeta=1} = 0 \tag{C.5}$$

This is the slope of the $m = m^0$ line as shown in Figure 7.1. Therefore $m = m^0$ line is the tangent to trajectory at limit state.

Appendix D

Derivation of m^0_{ref} Expression

m^0 (which is m^0_2) and m_L are obtained from linear elastic analysis at each iteration and $\zeta = \frac{m^0}{m_L}$. With respect to Figure 3.5 the m^0_{ref} expression is derived as follows:

m^0 reaches kinematically active reference volume based upper bound multiplier m^0_{ref}, when ζ reaches to $\zeta = 1+\sqrt{2}$. Therefore the ratio of m^0_{ref} and m^0 will be,

$$\frac{m^0_{ref}}{m^0_{B'}} = \frac{R^0_D}{R^0_{B'}} \tag{D.1}$$

Here, R^0_D is the R^0 value at $\zeta = 1+\sqrt{2}$ (shown in Figure 3.5).

$$\text{i.e. } R^0_D = \sqrt{2} \tag{D.2}$$

From the TBM curve, $R^0_{B'}$ is the R^0 value at $\zeta = \frac{m^0}{m_L}$ location. The expression for $R^0_{B'}$ can be expressed as ,

$$R^0_{B'} = \frac{1+\zeta^2}{2\zeta} \tag{D.3}$$

Substituting R^0_D and $R^0_{B'}$ in Eq. (D.1),

$$m^0_{ref} = \frac{\sqrt{2}m^0}{\frac{1+\zeta^2}{2\zeta}} \tag{D.4}$$

This is the expression for the kinematically active reference volume based upper bound multiplier.

Appendix E

Ansys Command Listing

```
/TITLE, Fixed Beam Elastic Analysis
! Beam Dimensions (m)

*SET,H,25.4E-3          !Height
*SET,D,25.4E-3          !Depth
*SET,Len,508E-3         !Length

! Loading

*SET,Prs,1.0E6          !Load: 1.0 MPa

! Material Model

*SET,YS,206.85E6        !Yield Strength
*SET,YM,206.85E9        !Young's Modulus
*SET,Pr,0.47            !Poisson's Ratio

! Enter preprocessor

/PREP7
ET,1,PLANE82,,,3        !Plane stress with thickness
R,THK,D                 !Depth of the beam is assigned
MP,EX,1,YM
MP,PRXY,1,Pr

! Modeling geometry

k,1,0
k,2,0,H/2
K,3,0,H
K,4,Len,0
K,5,Len,H/2
K,6,Len,H

L,1,2
L,2,3
L,1,4
L,4,5
L,5,6
L,6,3
L,2,5
```

```
AL,1,3,4,7
AL,7,5,6,2

! Meshing

*SET,M,30
*SET,Hdiv,(1/2)*m
*SET,Ldiv,20*m

LESIZE,1,,,Hdiv,1/1
LESIZE,2,,,Hdiv,1/1
LESIZE,4,,,Hdiv,1/1
LESIZE,5,,,Hdiv,1/1

LESIZE,3,,,Ldiv,1/1
LESIZE,7,,,Ldiv,1/1
LESIZE,6,,,Ldiv,1/1

AMESH,ALL

! Boundary conditions

DL,1,,ALL
DL,2,,ALL
DL,4,,ALL
DL,5,,ALL

! Loading

LSEL,S,LINE,,6
SFL,ALL,PRES,Prs
ALLSEL
SBCTRAN

FINISH

! Solving
/SOLU
ANTYPE,0
SOLVE
SAVE
FINISH

!Enter Postprocessor
/POST1
```

```
/TITLE, Single Stiffened Plate of Ship Structure
! Material model

*SET,YS,180e6                !Define Yield strength
*SET,YM,209E9                !Define Elastic Modulus
*SET,Pr,0.47                 !Define Poisson ratio

! Loading

*SET,Prs,100e3               !Applied Pressure

/prep7

ET,1,SOLID95                 !3D Solid Elements
MP,EX,1,YM
MP,PRXY,1,Pr

! Creating the Rectangular Plate

k,1,0,0,0
k,2,0,0.010,0
k,3,0.350,0.010,0
k,4,0.350,0.210,0
k,5,0.3165,0.210,0
k,6,0.3165,0.220,0
k,7,0.3915,0.220,0
k,8,0.3915,0.210,0
k,9,0.358,0.210,0
k,10,0.358,0.010,0
k,11,0.708,0.010,0
k,12,0.708,0,0
k,13,0,0,0
k,14,0,0,1


! Bottom portion

L,1,2
L,2,11
L,11,12
L,12,1
AL,1,2,3,4


! Middle portion
```

```
L,3,4
L,4,9
L,9,10
L,10,3
AL,5,6,7,8

! Top portion

L,5,6
L,6,7
L,7,8
L,8,5
AL,9,10,11,12

! Creating pseudo line for extruding

L,13,14
VDRAG,1,2,3,,,,13

! Deleting pseudo line
LDELE,13

! Dividing lines for meshing

LESIZE,14,,,9
LESIZE,19,,,9
LESIZE,17,,,35
LESIZE,21,,,35

LESIZE,22,,,15
LESIZE,27,,,15
LESIZE,29,,,3
LESIZE,25,,,3

LESIZE,30,,,3
LESIZE,35,,,3
LESIZE,33,,,20
LESIZE,37,,,20

! Along length

LESIZE,34,,,45
LESIZE,36,,,45
LESIZE,18,,,45
LESIZE,20,,,45
```

```
LESIZE,26,,,45
LESIZE,28,,,45
LESIZE,23,,,45
LESIZE,24,,,45

! Gluing the volumes to make connectivity

VGLUE,1,2,3
VSWEEP,2,2,13
VSWEEP,4,21,22
VSWEEP,5,25,26

FINISH

/SOLU

! Applying symmetry boundary condition

DA,4,SYMM
DA,6,SYMM

! Applying fixed boundary condition

DA,22,ALL
DA,13,ALL
DA,26,ALL

DA,21,SYMM
DA,2,SYMM
DA,25,SYMM

! Applying pressure load

SFA,7,1,PRES,Prs

SOLVE

FINISH

/POST1
```

```
/TITLE, Small Grillage of Ship Structure
!Material model

*SET,YS,180e6          !Define Yield strength
*SET,YM,209E9          !Define Elastic Modulus
*SET,Pr,0.47           !Define Poisson ratio

! Loading

*SET,Prs,100e3         !Applied Pressure

/prep7

ET,1,SOLID95
MP,EX,1,YM
MP,PRXY,1,Pr

! Creating the Rectangular Plate

k,1,0.380,0.010,0
k,2,0.380,0.210,0
k,3,0.3465,0.210,0
k,4,0.3465,0.220,0
k,5,0.4215,0.220,0
k,6,0.4215,0.210,0
k,7,0.388,0.210,0
k,8,0.388,0.010,0
k,9, 0.380,0,0
k,10,0.380,0,2

! Middle portion

L,1,2
L,2,7
L,7,8
L,8,1
AL,1,2,3,4

! Top portion

L,3,6
L,6,5
L,5,4
L,4,3
AL,5,6,7,8
```

```
! Creating pseudo line for extruding
L,9,10
VDRAG,1,2,,,,,9

!Deleting pseudo line
LDELE,9

! Top of T

LESIZE,25,,,4
LESIZE,21,,,4
LESIZE,23,,,10
LESIZE,18,,,10

! Other portion of T

LESIZE,17,,,3
LESIZE,18,,,3
LESIZE,10,,,30
LESIZE,15,,,30

! Along length of T

LESIZE,22,,,50
LESIZE,20,,,50
LESIZE,16,,,50
LESIZE,24,,,50
LESIZE,19,,,50
LESIZE,11,,,50

! Array of volumes

VGEN,3,all, , ,0.358, , , ,0

! Creating the rest of the model

k,101,0,0,0
k,102,0,0.1,0
k,103,0.03,0.1,0
k,104,0.03,0,0
k,105,0,0,0
k,106,0,0,2

L,101,102
L,102,103
```

```
L,103,104
L,104,101
AL,73,74,75,76

! Creating pseudo line
L,105,106

VDRAG,37,,,,,,77

! Deleting pseudo line

LDELE,77

! Division of side portion

LESIZE,81,,,6
LESIZE,85,,,6
LESIZE,78,,,20
LESIZE,83,,,20

! Along length of side portion

LESIZE,82,,,50
LESIZE,84,,,50
LESIZE,79,,,50
LESIZE,80,,,50

! Array of rest of the volumes

VGEN,2,7, , ,1.454, , , ,0

! Creating the bottom block

BLC4,0.03,0,1.424,0.01,2


! Gluing the volumes to make connectivity

VGLUE,ALL

LESIZE,137,,,132
LESIZE,130,,,30
LESIZE,17,,,4
LESIZE,132,,,30
LESIZE,36,,,4
```

```
LESIZE,134,,,30
LESIZE,60,,,4
LESIZE,136,,,30
LESIZE,116,,,4
LESIZE,111,,,4

! Along length of side portion

LESIZE,107,,,50
LESIZE,88,,,50
LESIZE,108,,,50
LESIZE,84,,,50

! Meshing

VSWEEP,1,7,1
VSWEEP,3,18,17
VSWEEP,5,30,29


VSWEEP,12,66,65
VSWEEP,13,70,69
VSWEEP,14,74,73
VSWEEP,15,81,80
VSWEEP,10,58,57
VSWEEP,11,62,61

FINISH


/SOLU

!Applying fixed boundary condition

DA,58,ALL
DA,57,ALL

DA,62,ALL
DA,61,ALL

DA,81,ALL
DA,80,ALL

DA,66,ALL
DA,65,ALL
```

```
DA,7,ALL
DA,1,ALL

DA,70,ALL
DA,69,ALL

DA,18,ALL
DA,17,ALL

DA,74,ALL
DA,73,ALL

DA,30,ALL
DA,29,ALL

! Applying pressure load

SFA,46,1,PRES,Prs
SFA,41,1,PRES,Prs
SFA,79,1,PRES,Prs

SOLVE

FINISH

/POST1
```

/TITLE, Large Grillage of Ship Structure

```
! Material model

*SET,YS,180e6          !Define Yield strength
*SET,YM,209E9          !Define Elastic Modulus
*SET,Pr,0.47           !Define Poisson ratio

! Loading

*SET,Prs,100e3         !Load = 100e3

/prep7

ET,1,SOLID92
MP,EX,1,YM
MP,PRXY,1,Pr

! Creating the Rectangular Plate

k,1,0.380,0.010,0
k,2,0.380,0.210,0
k,3,0.3465,0.210,0
k,4,0.3465,0.220,0
k,5,0.4215,0.220,0
k,6,0.4215,0.210,0
k,7,0.388,0.210,0
k,8,0.388,0.010,0
k,9, 0.380,0,0
k,10,0.380,0,3.018

! Middle portion

L,1,2
L,2,7
L,7,8
L,8,1
AL,1,2,3,4

!Top portion

L,3,6
L,6,5
L,5,4
L,4,3
```

```
AL,5,6,7,8
! Creating pseudo line for extruding

L,9,10

VDRAG,1,2,,,,,9

! Deleting pseudo line

LDELE,9

! Array of volumes

VGEN,3,all, , ,0.358, , , ,0


! Creating the rest of the model

k,101,0,0,0
k,102,0,0.1,0
k,103,0.03,0.1,0
k,104,0.03,0,0
k,105,0,0,0
k,106,0,0,3.018

L,101,102
L,102,103
L,103,104
L,104,101

AL,73,74,75,76

! Creating pseudo line
L,105,106

VDRAG,37,,,,,,77

! Deleting pseudo line

LDELE,77


! Array of rest of the volumes

VGEN,2,7, , ,1.454, , , ,0
```

```
! Creating the bottom block

BLC4,0.03,0,1.424,0.01,3.018

! Gluing the volumes to make connectivity

VGLUE,ALL

! Creating transverse member

! Top portion
BLOCK,-0.468,1.952,0.335,0.353,1.949,2.069

! Bottom portion (part 1)
BLOCK,-0.468,-0.175,0.01,0.335,2,2.018

! Copying Bottom portion (part 1)

VGEN,2,4, , ,2.127, , , ,0

! Bottom portion (part 2)
BLOCK,-0.175,0.205,0.01,0.335,2,2.018
VSBV,7,10,,DELE,KEEP

! Copying Bottom portion (part 2)

VGEN,2,8, , ,1.454, , , ,0

! Bottom portion (part 3)

BLOCK,0.205,0.563,0.01,0.21,2,2.018
VSBV,9,1,,DELE,KEEP

BLOCK,0.205,0.563,0.21,0.335,2,2.018
VSBV,9,12,,DELE,KEEP

! Copying Bottom portion (part 3)

VGEN,3,16, , ,0.358, , , ,0
VGEN,3,17, , ,0.358, , , ,0
VGEN,3,18, , ,0.358, , , ,0

VGLUE,16,17,18
VGLUE,9,22,20
VGLUE,19,23,21
```

```
VGLUE,ALL

!Meshing
ESIZE,0.03
MSHKEY,0
VMESH,ALL

FINISH

/SOLU

! Applying fixed boundary condition

DA,7,SYMM
DA,1,ALL

DA,18,SYMM
DA,17,ALL

DA,30,SYMM
DA,29,ALL

DA,66,SYMM
DA,65,ALL

DA,70,SYMM
DA,69,ALL

DA,74,SYMM
DA,73,ALL

DA,58,SYMM
DA,57,ALL

DA,62,SYMM
DA,61,ALL

DA,81,SYMM
DA,80,ALL

DA,40,ALL
DA,51,ALL

DA,231,ALL
DA,230,ALL
```

```
! Applying pressure load

SFA,46,1,PRES,Prs
SFA,41,1,PRES,Prs
SFA,79,1,PRES,Prs

SOLVE

FINISH

/POST1
```

! Post-Processing Macro for EMAP and Limit Load Multipliers

```
*ask,NI,Required Number Of Iterations,1
*ask,q,Enter the 'q'val 1 for plane strain and 2 for plane stress,1
!NI _ number of iterations to be run
!Input the number of iterations to be run

*dim,enub,array,nd2,nd1          !Defining an array for writing the element numbers.
*get,ecou,elem,0,count
*dim,eval,array,ecou,NI+1        !Def Eval array
*vfill,eval(1,1),ramp,YM,0
*dim,ests,array,ecou,5           !Defining array for element stress.
*dim,ests2,array,ecou,5
*dim,vol,array,ecou,1


!getting the centroidal location of the elements

*dim,loe,array,ecou,3
*do,lo,1,ecou,1
*get,loe(lo,1),elem,lo,cent,x
*get,loe(lo,2),elem,lo,cent,y
*get,loe(lo,3),elem,lo,cent,z
*enddo

tvol=0
*do,v,1,ecou,1                   !Reading volumes of each element and summing
them up.
*get,vol(v,1),elem,v,volu
tvol=tvol+vol(v,1)
*enddo

*do,gp,1,NI,1
sp=gp+1


etable,sigc,s,eqv                !Reading stress into element table.
etable,sot,s,eqv                 !Sorting of element stresses.
esort,etab,sot,0,0
*get,meqs,sort,0,max
etable,eqst,epto,eqv             !Reading strain values into element table.

trn=0                            !Calculation of reference stress.
*do,k,1,ecou,1
*get,els,etab,1,elem,k
```

```
rn=els*els*vol(k,1)
trn=trn+rn
*enddo
srv=(trn/tvol)
sr=sqrt(srv)


! finding out the multiplyer values

ML=ys/meqs                    ! Calculation of lower bound multiplier

MUN2=0
MUD2=0

M01D2=0
M01D=0
M01N2=0
M01N=0

M02N2=0
M02N=0
M02D2=0
M02D=0

*do,z,1,ecou,1
*get,elsa,etab,1,elem,z
*get,elst,etab,3,elem,z

MUN1=elst*vol(z,1)            !Calculation of upper bound multiplier
MUN2=MUN2+MUN1
MUD1=elsa*elst*vol(z,1)
MUD2=MUD2+MUD1

M01N1=vol(z,1)
M01N2=M01N2+M01N1
M01D1=vol(z,1)*elsa**2        !Calculation of M01 multiplier
M01D2=M01D2+M01D1

M02N1=vol(z,1)/eval(z,gp)     !Calculation of M02 multiplier
M02N2=M02N2+M02N1
M02D1=elsa*elsa*vol(z,1)/eval(z,gp)
M02D2=M02D2+M02D1


*enddo
```

```
MU=ys*MUN2/MUD2

M01N=sqrt(M01N2)
M01D=sqrt(M01D2)
M01=ys*M01N/M01D


M02N=sqrt(M02N2)
M02D=sqrt(M02D2)
M02=YS*M02N/M02D

*SET,JETA,(M02/ML)
*SET,Tan_theta,0.2929                !Slope of tangent

*if,JETA,LE,(1+sqrt(2)),then
m_tangent = m02/(1+(Jeta-1)*Tan_theta)
*endif

*if,JETA,GT,(1+sqrt(2)),then
cee=0.2929*(JETA-1)
JETAF=(1+cee)+sqrt(((1+cee)*(1+cee))-1)
m_tangent = M02/(1+(Jetaf-1)*Tan_theta)
*endif


!*cfopen,MULT%gp%                    !Writing out the multipliers
*cfopen,Iter,,,append
*vwrite,gp
(f9.4)
!(1x,'ITERATION NO : ',f9.4)
*cfopen,MULT_ML,,,append
*vwrite,ML
(f9.4)
!(1x,'Multiplier ML : ',f9.4)
*cfopen,MULT_MAT,,,append
*vwrite,m_tangent
(f9.4)
!(1x,'Multiplier MAT : ',f9.4)
*cfopen,MULT_M01,,,append
*vwrite,M01
(f9.4)
!(1x,'Multiplier M01 : ',f9.4)
*cfopen,MULT_M02,,,append
*vwrite,M02
(f9.4)
```

```
!(1x,'Multiplier M02 : ',f9.4)
!*cfclos

*cfopen,MULT_MU,,,append
*vwrite,MU
(f9.4)
(1x,'Multiplier MU : ',f9.4)
*cfclos


*do,k,1,ecou,1
*get,ests(k,1),etab,1,elem,k
*enddo

*cfopen,ESTS%gp%                        !Opening a file to write element stress.
*do,k,1,ecou,1
*get,elsts,etab,1,elem,k
*set,ymv,eval(k,gp)
*set,volu,vol(k,1)
*set,lx,loe(k,1)
*set,ly,loe(k,2)
*set,lz,loe(k,3)
*vwrite,k,elsts,volu,ymv,lx,ly,lz       !Writing element stresses to a ESTS1 file.
(1x,'Element No : ',f6.0,3x,'Stress Value : ',f9.4,3x,'Volume : 'f11.3,3x,'YModule Value :
',e21.10,2x,'LOE : 'f11.4,2x,f11.4,2x,f11.4)
*enddo
*cfclos

*do,c,1,ecou,1                  !deninig the values of eval.
*set,eval(c,gp+1),eval(c,gp)
*enddo


!****EMAP PART****

*do,m,1,ecou,1
ests(m,3)=sr/ests(m,1)                  !Dividing limit stress with individual
ests(m,4)=(ests(m,3)**q)                !Elastic Adjustment parameter
eval(m,gp+1)=eval(m,gp)*ests(m,4)       !Multiplying above obtained fraction with
*enddo


/quit
/prep7
```

```
*do,x,1,ecou,1
mp,ex,x,eval(x,gp+1)
*if,gp,eq,1,then
mp,prxy,x,0.47
*endif                                  ! Creating material property
emodif,x,mat,x
*enddo

/quit
/solu
solve
/quit
/post1

*enddo
```